Chemical Approaches to Understand the On-Membrane Action of Magainin 2

Author: Nanjun Liu

Boston College

The Graduate School of Arts and Sciences

Department of Chemistry

CHEMICAL APPROACHES TO UNDERSTAND THE ON-MEMBRANE ACTION OF MAGAININ 2

a thesis

by

NANJUN LIU

submitted in partial fulfillment of the requirements

for the degree of

Master of Science

August 2011

Chemical Approaches to Understand the On-Membrane Action of Magainin 2

By: Nanjun Liu

Advisor: Jianmin Gao

Abstract

There is substantial interest in exploring antibiotic alternatives with a new mode of action due to the increasing rates of bacterial resistance against current antibiotics. Antimicrobial peptides (AMPs) may take up the battle against bacteria in the future because as a result of their membrane-lysis mechanism, it is more difficult for bacteria to develop resistance against AMPs. Although AMPs could preferentially bind to and disrupt negatively charged bacterial membranes through electrostatic and hydrophobic interactions, there is still a great need to further increase the potency and selective toxicity towards bacteria for clinical applications. Herein, we present two strategies to improve the selectivity: light activation and environment-responsive moiety incorporation. Along the way, we also explored the effect of structure stabilization on AMPs action. A well-characterized antimicrobial peptide magainin 2 (mag2) was used as a prototype. Chemical manipulations of mag2 sequence were achieved by incorporation of unnatural amino acids. The selectivity was then tested on liposomes as a membrane model, as well as on bacterial cells and human red blood cells (hRBCs). Different extents of selectivity enhancement were observed from the modified peptides, and within the attempts to illustrate these results, we have gained useful information revealing the membrane-lysis mechanism, which may help us to rationally design and engineer AMPs as therapeutic drugs in the future.

Acknowledgement

I would like to thank my advisor, Dr. Gao, for guidance and support through my graduate studies. Thank you for understanding and supporting my decision to take a different step from my original plan. It is a valuable experience to work with you on these exciting projects, and this experience would definitely play an important role in my future career.

I would also like to thank the Gao group members. We all together created this energetic group. Thank Hong Zheng and Fang Wang for your help on the discussions about research as well as my thesis. Thank Christopher Pace for your suggestions on my thesis also. And thank Luoheng Qin for your guidance and help on the organic synthesis part of my work. Thanks for the help of Chris Sheridan to synthesize one of the unnatural amino acids. Thanks to all my friends in Boston College, I had this great life in BC because of you. Thank you to Dale Mahoney for all of your help and time during this period.

Thanks a billion to Xixi Sun, thank you for always having your faith in me and being my strongest backup. I wouldn't make this far without you. Great thanks to my parents, thank you for supporting every decision I make and the way I choose to live my life.

Table of Contents

List of Figures

List of Tables

List of Schemes

List of Abbreviations

AMPs	Antimicrobial peptides
Arg	Arginine
CD	Circular dichroism
DCM	Dichloromethane
DLS	Dynamic light scattering
DPC	n-dodecylphosphocholine
Et_2O	Diethyl ether
EtOAc	Ethyl acetate
Fmoc	Fluorenylmethyloxycarbonyl
HCl	Hydrogen chloride
hRBS	human red blood cells
LC-MS	Liquid chromatography–mass spectrometry
LHA	Lutidinoxylalanine
Lys	Lysine
LUVs	Large unilamellar vesicles
Mag2	Magainin 2
M	Molar
MeCN	Acetonitrile
MeOH	Methanol
Na_2SO_4	Sodium sulfate

NBD-POPE	1,2-dioleoyl-sn-glycero-3-phosphoethanolamine-N-(7-nitro-2-1,3-benzoxadiazol-4-yl)
PAP	phenyl-azophenylalanine
Phe	Phenylalanine
Pra	Propargylglycine
POPC	1-palmitoyl-2-oleoyl-*sn*-glycero-3-phosphocholine
POPG	1-palmitoyl-2-oleoyl-*sn*-glycero-3-phospho-(1'-*rac*-glycerol)
RP-HPLC	Reverse-phase high performance liquid chromatography
SEC-HPLC	Size-exclusion high performance liquid chromatography
SDS	Sodium dodecyl sulfate
SPPS	Solid-phase peptide synthesis
SUVs	Small unilamellar vesicles
TFE	Trifluoroethanol
THF	Tetrahydrofuran
Triton X-100	Octylphenoxypolyethoxyethanol
Trp	Tryptophan
UV/Vis	Ultraviolet/visible light spectroscopy

Chapter 1: Introduction

1.1 Global problem of antibiotic resistance

Since their discovery, antibiotics have been the most useful weapons in fighting bacterial infections throughout the world. For example, penicillin, developed by Alexander Fleming in 1928 and once called a "miracle drug", has defeated many once-fatal bacterial infections and saved countless lives. However, it is a natural ability of bacteria to develop resistance against antibiotics, and the process of antibiotic resistance development has even been accelerated by the indiscriminate use of antibiotics in farm animals as well as people. According to the data from World Health Organization (WHO), every year in the European Union alone, about 25,000 patients die because of serious resistant bacterial infections acquired in hospitals. Because of this continuously growing problem, the WHO has set antibiotic resistance as the theme of World Health Day 2011 and called on the whole society to take action on regulation of proper antibiotics use and more importantly, exploration of new antibiotic medicines.

This worldwide problem has thus stimulated the interest in developing alternatives for traditional antibiotics, especially those with the ability of bypassing current resistance mechanism. Ideally, these alternatives should be as natural as possible, with a wide range of action over several pathogens, easy to produce, and not prone to induce resistance[1]. Accumulated studies have proven that antimicrobial peptides (AMPs), isolated from a wide range of organisms and species from bacteria to humans, might

[1] Zasloff, M., Antimicrobial peptides of multicellular organisms. *Nature* **2002**, *415*, 389-395

serve as promising replacements for eliminating pathogenic bacteria that are increasingly resistant to current antibiotic treatment.

1.2 Antimicrobial peptides as an alternative to antibiotics

Antimicrobial peptides (AMPs) are evolutionarily conserved components of organisms and are found among all types of life[2]. As effectors of innate immunity, AMPs directly kill a broad spectrum of microbes, including Gram-positive and Gram-negative bacteria, fungi, and certain viruses[3]. Since the first class of antibacterial peptides, cecropins were identified by Steiner 1981[4], the number of AMPs discovered has increased at a rapid pace. By August 2011, more than 1700 of AMPs have been identified according to the Antimicrobial Peptides Database (APD: http://aps.unmc.edu/AP/main.php). Despite the diversity of peptide sequence, AMPs have several properties in common. Most AMPs are short in length with 5 to 40 amino acid residues. Generally, AMPs are amphipathic, which enables them to selectively interact with and disrupt lipid membranes. The largest group of AMPs contains cationic peptides widely distributed in animals and people. The positive charges are usually provided by Lys and Arg, along with ~30% or more hydrophobic residues such as Trp and Phe.

Two key features of AMPs contribute to their potential as antibiotics alternatives[5]. (1) It is much less likely for bacteria to develop resistance against AMPs because of their distinctive mechanism of action. (2) AMPs could selectively target and kill bacterial

---

[2] Marshall, S.H. *Electronic Journal of Biotechnology* **2003**, *6*, 271-284.
[3] Gomesa, V.M.; Carvalhoa, A.O.; Cunhab, M. Da; Kellera, M.N.; Jr.c, C. Bloch; Deolindod, P.; Alvesd, E.W. *Toxicon* **2005**, *45*, 817–827.
[4] Steiner, H.; Hultmark, D.; Engstro¨m, A.; Bennich, H.; Boman, H.G. *Nature* **1981**, *292*, 246–248.
[5] Matsuzaki, K. *Biochimica et Biophysica Acta* **1999**, *1462*, 1-10.

cells.

1.3 Mechanism of antimicrobial action

Although the detailed mechanism of AMPs action may vary among different peptides, the membrane-targeting mechanism is the most conserved killing mechanism of AMPs. There is a general mechanism – the Shai-Matsuzaki-Huang (SMH) model (Figure 1) that explains the activity of most AMPs[6,7]. To simplify this process, the mechanism can be divided into two steps. Firstly, the peptide will partition into the membrane-water interface with concomitant folding to afford an amphipathic structure. A combination of electrostatic forces and hydrophobicity drives the association between peptide and membrane, and determines the binding affinity of peptides. The second step involves membrane permeabilization or on-membrane action of the bound peptides, of which the molecular events remain vaguely defined. For most AMPs we are interested in, there is a threshold peptide to lipid ratio P/L^*[8]. When P/L is below P/L^*, peptides will impose positive curvature strain on the membrane by expanding the polar head group region to form the 'toroidal' pore, and peptides can translocate into the inner leaflet upon disintegration of the pore as shown in b-d of the SMH model (Fig. 1)[9]. As P/L increases above P/L^*, stable pores are detected in the membrane[10], or complete disruption of the

---

6 Yang, L.; Weiss, T. M.; Lehrer, R. I. & Huang, H. W. *Biophys. J.* **2000**, *79*, 2002-2009.

7 Shai, Y. *Biochim. Biophys. Acta* **1999**, *1462*, 55-70.

8 Huang, H.W. *Biochemistry*, **2000**, *39*, 139-145

9 Matsuzaki, K.; Nakamura, A.; Murase, O.; Sugishita, K.; Fujii, N.; Miyajima, K. *Biochemistry*, **1997**, *36*, 2104-2111

10 Huang, H.W. *Biochimica et Biophysica Acta* **2006**, *1758*, 1292-1302

membrane in a detergent-like way happens for a few peptides[11,12](d-f in Fig. 1).

Additionally, hypotheses have been proposed to explain the mechanisms by which peptides kill target cells other than membrane lysis; such hypotheses include induction of hydrolases which degrade the cell wall, disturbance of membrane functions, and damage to crucial intracellular targets after internalization of the peptide[1].

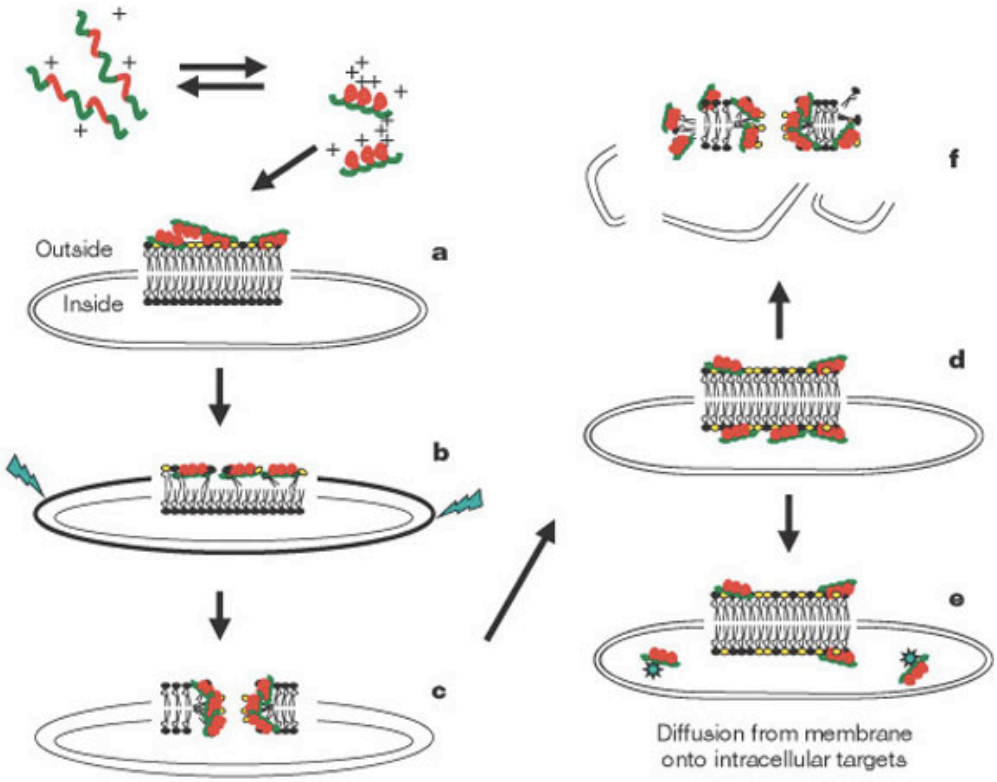

Figure 1. The Shai-Matsuzaki-Huang model of the mechanism of antimicrobial action (adapted from [1])

Bacteria can readily develop resistance against traditional antibiotics; however, it is much harder for them to build resistance against AMPs. Antibiotics are designed to

11 Shai, Y. Biopolymers 2002, *66*, 236-248.

12 Bechinger, B.; Lohner, K. BBA Biomembranes 2006, *1758*, 1529-1539

fight bacteria by targeting specific parts of the bacteria's structure or cellular machinery. There are four major mechanisms (Fig. 2) that bacteria exhibit resistance against antibiotics[13]: altering the target site to which antibiotics bind; upregulating pumps that expel antibiotics from the cell; producing enzymes that inactivate or modify antibiotics; producing an alternative target that "bypasses" the effect of antibiotics. The rapid reproduction of bacteria (as little as 20 min) and the steady evolution of resistant bacteria have resulted in a situation that almost all antibiotics have lost their effectiveness against targeted bacteria over time. For example, in 1947-only four years after penicillin started being mass-produced, *Staphylococcus aureus* was found to be one of the bacteria in which penicillin resistance was developed. Now nearly all strains of *Staphylococcus aureus* in the United States are resistant to penicillin, and since 1996, strains of *S. aureus* have been reported to be decreasingly susceptible to vancomycin, which has been the only effective treatment left.

One the other hand, because the target of AMPs is the bacterial membrane, to avoid such attack, bacteria will have to change their membrane composition, lipid arrangements, which is probably a "costly" way for most bacteria[1]. AMPs have remained effective against bacterial infections for 10^8 years, despite their continual presence in the bacterial environment, which could be a strong indication that the resistance of bacteria against AMPs is difficult to evolve in the short term[1]. Additionally, the diversity of AMPs sequence and structure, and the varied modes of action might impede the development of resistance. This feature plays an important role in the determination of

[13] Hawkey, P.H. *BMJ*, **1998**, *317*, 657-660

AMPs as attractive antibiotic alternatives and encourages exploration of new therapeutic drugs using AMPs as a model.

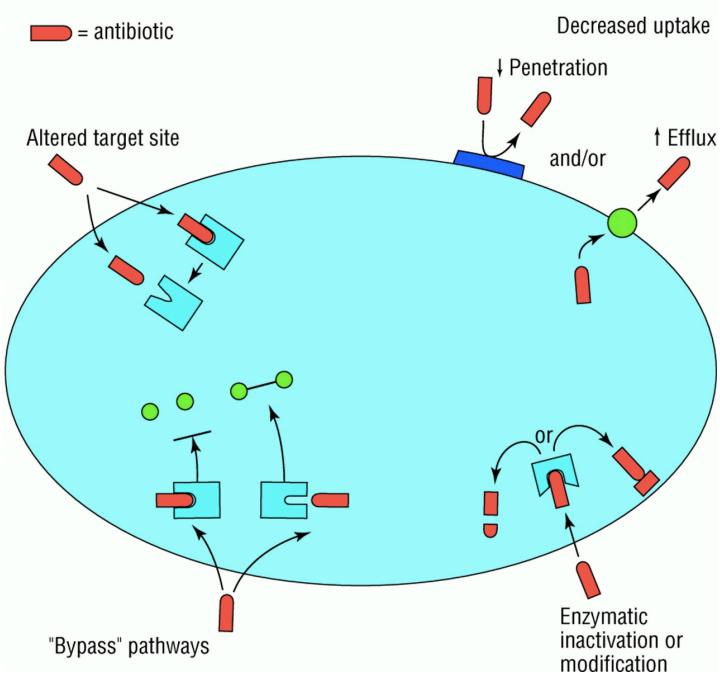

Figure 2. Four major biochemical mechanisms of antibiotic resistance (Adapted from [13])

1.4 Selective toxicity against bacteria

Besides their unique mechanism of action, the intrinsic selective toxicity of AMPs against bacteria is another key feature that makes AMPs stand out as antibiotic drugs. The difference in the membrane composition between eukaryotic and prokaryotic cells accounts for the ability of AMPs to kill bacteria selectively. For mammalian cells, the outer leaflet is composed principally of phosphatidylcholine (45-55%) and sphingomyelin, which are both neutral, zwitterionic phospholipids. Also ~30% of the neutral sterol cholesterol exist in the mammalian plasma membrane outer leaflets. In contrast, the typical bacterial phospholipids in the outer leaflet of the bilayer are

negatively charged lipids (20-25%) such as cardiolipin (CL) and phosphatidylglycerol (PG) with phosphatidylethanolamine as the zwitterionic component.

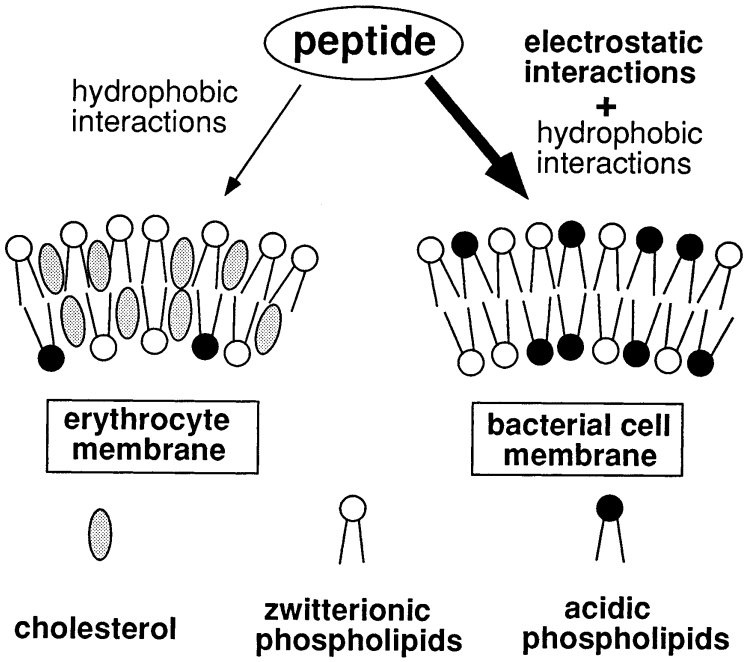

Figure 3. Molecular basis for membrane discrimination by AMPs (Adapted from [5])

There are two main interactions between peptides and bacterial membranes: hydrophobic interactions between the non-polar amino acids and the hydrophobic core of the membrane[5], and electrostatic interactions between cationic amino acid residues and negatively charged phospholipid headgroups. The hydrophobicities of AMPs are usually too low to effectively interact with neutral membranes, avoiding toxicity towards

mammalian cells, thus electrostatic interactions play a regulatory role in differentiating microorganisms from eukaryotic cells (Figure 3).

1.5 Experimental goals

For AMPs to fulfill their therapeutic promise as the next generation of antibiotic drugs, more studies are needed to improve their properties such as enhanced selectivity (reduce the potential for unwanted toxicity) and increased antimicrobial activity. Additionally, detailed information about their mechanisms of action is meaningful towards rational design and engineering of AMPs. Here we present three related projects aiming to enhance the selectivity while at the same time, obtaining useful information towards elucidation of the mechanism.

Chapter 2: Experiments and Results

2.1 Overview of magainin 2

Magainins, first discovered in the skin of *Xenopus laevis*[14,15], are a series of cationic peptides with 21 to 27 amino acid residues that create an amphiphatic secondary structure. Magainins show a broad spectrum of antimicrobial activity, killing not only Gram-negative and –positive bacteria, but also fungi and protozoa. As a 23-residue cationic antimicrobial peptide (GIGKFLHSAKKFGKAFVGEIMNS), Magainin 2 (Mag2) might be the most studied among all the AMPs. It is unstructured in aqueous

[14] Zasloff,M. *Proc.Natl.Acad.Sci*.**1987**, *84*, 5449-5453.
[15] Matsuzaki, K. *Biochim.Biophys.Acta*, **1998**, *1376*, 391-400

solution but forms an α-helix upon contact with the membrane, characterized by separated cationic and hydrophobic faces. Fig. 4 is a helical wheel projection of mag2 clearly showing a hydrophobic face and hydrophilic face separated from each other[16]. The three Phe residues are important components of the hydrophobic face, and four Lys residues contribute to the overall positive charge of the peptide.

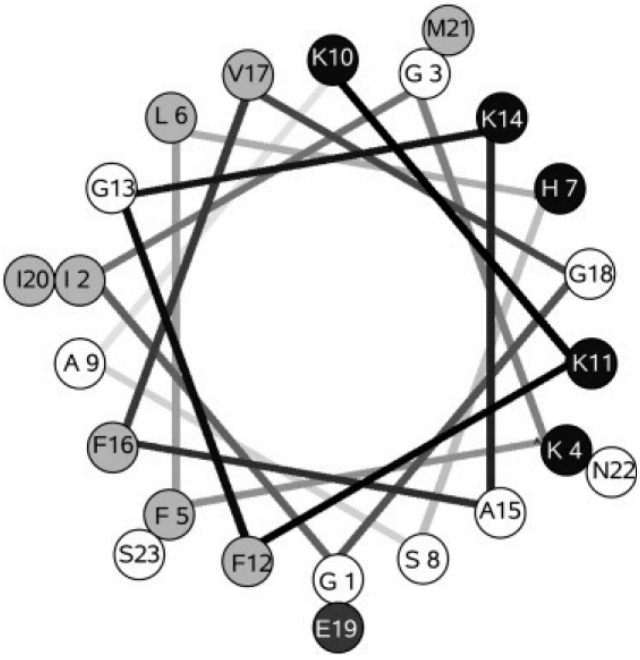

Figure 4. Helical wheel projection of Mag2. Dark shading, acidic residues; light shading, hydrophobic resiudes; and open symbols, hydrophilic residues (adapted from [16])

Extensive studies on the development of potent drugs based on mag2 have been performed, such as structure-activity relationship[17,18,19,20,21,22,23]. Various structural

---

16 Gregory S.M.; Pokorny A.; Almeida P.F. *Biophys J.* **2009***, 96*, 116-31.
17 Zasloff, M.; Martin, B.; Chen, H. *Proc. Natl. Acad. Sci.,* **1988**, *85*, 910-913
18 Chen, H.; Brown, J.H.; Morell, J.L.; Huang, C.M. *FEB*, **1988***, 236*, 462-466
19 Matsuzaki, K.; Sugishita, K.; Harada, M.; Fujii, N.; Miyajima, K. *Biochimica et Biophysica Acta* **1997**, *1327*, 119-130

parameters such as α-helicity, net positive charge, hydrophobicity and hydrophobic moment are related to mag2 antimicrobial activity. The importance of an amphiphathic α-helical structure and a net positive charge for antimicrobial activity has been emphasized by these studies. Replacement of a low helix propensity amino acid with a high propensity Ala not only increased the α-helicity, but also antimicrobial activity[18]. An increase in peptide positive charge enhanced the bactericidal activity[19, 21]. Hydrophobicity enhancement is also a method of intensifying the antimicrobial potency, however, this type of method simultaneously raised the toxicity[22].

2.2 Photocontrolling magainin 2 antimicrobial activity

2.2.1 Background and experimental design

Light regulation of bio-systems is of considerable interest because light can be readily tuned and focused, and spatial and temporal control can be utilized to provide "on-command" activation. Caged bioactive molecules could be activated by release of a chemical blocking group with a light pulse as the external stimuli[24]. However, this process is irreversible and people are more interested in utilizing reversible photo-control over bioactive compounds. To this end, an azobenzene-based cross-linker was

[20] Cuervo, J.H.; Rodriguez, B.; Houghten, R.A. *Peptide research*, **1988**, *1*, 81-86
[21] Bessalle, R.; Haas, H.; Goria, A.; Shalit, I.; Fridkin, M.; *Antimicrobial Angents and Chemotherapy*, **1992**, *36*, 313-317
[22] Dathe, M.; Wieprecht, T.; Nikolenko, H.; Handel, L.; Maloy, W.L.; MacDonald, D.L.; Beyermann, M.; Bienert, M. *FEBS Letters*, **1997**, *403*, 208-212
[23] Maloy, W.L.; Kari, U.P. *Biopolymers*, **1995**, *37*, 105-122
[24] Nguyen, A.; Rothman, D.M.; Stehn, J.; Imperiali, B.; Kramer, R.H. Nat. Biotechnol. **2004**, *22*, 993-1000

successfully applied to optically control peptide helix content in a reversible manner[25]. Also, incorporation of the photoisomerizable amino acid phenyl-azophenylalanine (PAP) into enzyme structures has been utilized to create photoswitching enzyme activities[26, 27]. Azobenzene can be switched between *trans* and *cis* conformations with appropriate wavelengths of light (Figure 5). Irradiation with ~340nm light converts azobenzene from *trans* to *cis* isomer; the *cis* conformation slowly relaxs back to the *trans* conformation in the dark [$t_{1/2}$≈3 days][28] or upon irradiation at ≥420nm[29]. Because of significant difference between the two isomers in geometry and dipole moments, remarkable effects have been observed with azobenzene-modified peptides and proteins, including photoinduced helix-coil transitions, helix sense reversal, and aggregation/disaggregation[30]. Inspired by these studies, we incorporated PAP into the sequence of mag2. We hypothesized that the *cis*/*trans* isomerization of azobenzene could be utilized to tune the membrane-lytic activity of Mag2.

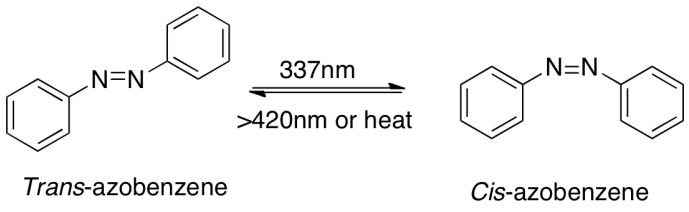

Figure 5. Isomerization of azobenzene moiety

---

25 Woolley, G.A. Acc. Chem. Res. **2005**, *38*, 486-493

26 Willner, I.; Rubin, S. and Riklin, A. *J. Am. Chem. Soc*. **1991**, *113*,3321.

27 Liu, D.; Karanicolas, J.; Yu, C.; Zhang, Z.; Woolley, G.A. *Bioorg. Med. Chem. Lett.* **1997**, *7*, 2677-2680

28 Zhang, J.; James, D. A.; Woolley, G.A. *J. Peptides Res*.**1999**, *53*, 560-56.

29 Zimmerman, G.; Chow, L.Y.; Paik, U.J., *J. Am. Chem. Soc.* **1958**, *80*, 3528-3531

30 Pieroni, O.; Fissi, A.; Angelini, N.; Lenci, F., Photoresponsive polypeptides. *Acc. Chem. Res*. **2001**, *34*, 9-17

2.2.2 Results and Discussions

To test this hypothesis, we synthesized a mag2 variant (F12PAP-mag2) with Phe12 replaced by PAP. Phe12 is at the center of the peptide sequence, so when the peptide forms an α-helix upon association with the membrane, the azobenzene moiety will be located in the center of helical structure which will allow for maximum structural change with the *cis*/*trans* isomerization. We first studied the reversible *trans*-to-*cis* photoisomerization under irradiation with light of 337nm (Fig. 6), and the obtained *cis*-isomer had completely different UV-vis spectra from its corresponding *trans* counterpart. The photostationary equilibrium (*cis*/*trans*=80:20, evaluated by LC-MS) was reached within 1 hr. Alternatively, when exposed to light of longer wavelength (>400nm), the *cis* form was converted to predominantly the *trans* conformation.

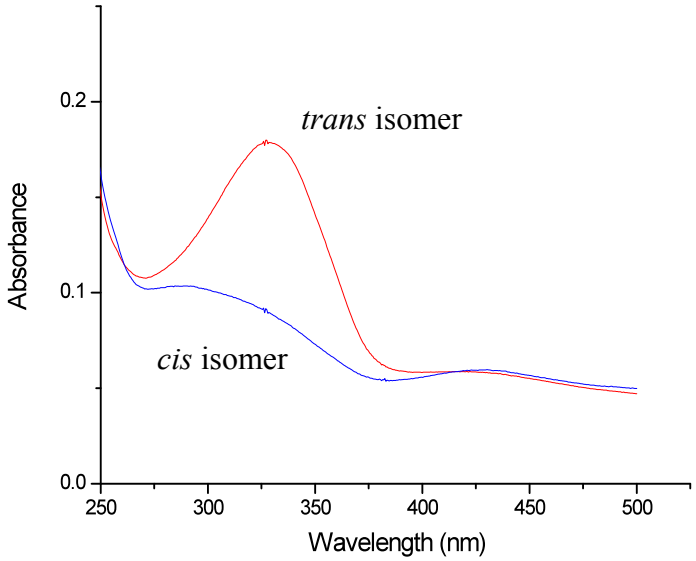

Figure 6. Absorption spectra of F12PAP-Mag 2 (4μM) in 3M GdnCl, 10mM TES, 100mM sodium citrate, pH 7.0 buffer: irradiation at 337 nm for 1 hr converted the *trans* isomer to the *cis* isomer

Next, we investigated the membrane-lytic activity of F12PAP-mag2 against large unilamellar vesicles (LUVs) by utilizing an optimized liposome leakage assay with Tb^{3+} encapsulated vesicles[31, 32] (see Materials and Methods, Scheme S9).

Peptides were titrated into solutions containing dipicolinic acid (DPA) and negatively charged LUVs (POPC/POPG 1/1) encapsulating with 50 mM $TbCl_3$ inside the vesicles. Membrane lysis by mag2 variants caused the leakage of Tb^{3+}, which then formed luminescent complexes with the DPA in the solution. F12PAP-mag2 was highly potent in lysing LUVs when it adopted the *trans* conformation (Fig. 7), and irradiation at 337nm afforded predominantly the *cis* isomers that showed around a 5-6 fold decrease in membrane-lytic activity. The incomplete *trans* to *cis* transition may contribute to the observed activity of "*cis*" isomer, and the difference in membrane-lytic activity between *trans* and *cis* peptides may be even larger by taking this into consideration. Notably, the membrane-lytic activity could be fully recovered either by irradiation at a longer wavelength (>400nm) or dark incubation.

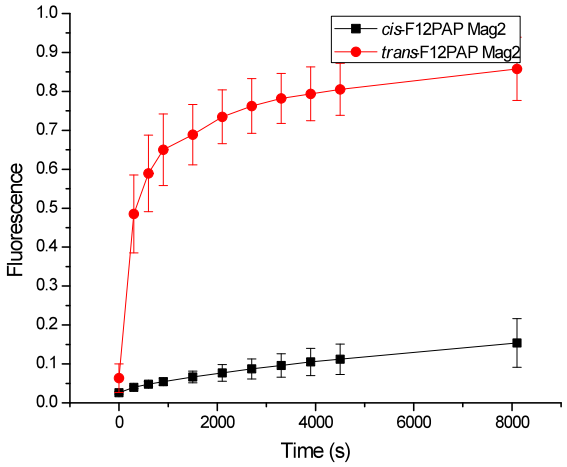

Figure 7. Photoswitching modulates mag2 membrane permeabilization. Isomerization of azobenzene elicites a significant change in membrane lysis. This experiment was performed with 2 μM peptide and 500 μM LUVs made of POPC/POPG 1/1 at room temperature with stirring. (Data presented is average of three measurements)

[31] Rathinakumar, R.; Wimley,W.C. *J.Am.Chem.Soc.,* **2008**, *130*, 9849-9858.

[32] Rausch, J.M.; Wimley,W.C. *Anal.Biochem.*, **2001**, *293*, 258-263

Antimicrobial activities of AMPs are usually modified in two aspects corresponding to the two steps of the SMH model: binding affinity and membrane-disturbing ability of bound peptides. One of them or both could be altered upon azobenzene photoisomerization.

To address this question, we incorporated a dansyl (DNS) group in addition to the azobenzene group into mag2 to obtain another variant F5DNS-F12PAP-mag2 (see Materials and Methods, Scheme S8). Dansyl was used as an environment-sensitive fluorescent probe to detect the association between F5DNS-F12PAP-mag2 and lipid bilayers. When the peptides labeled with dansyl bind to membrane, dansyl fluorescence is blue-shifted from 545nm to 503nm, with the intensity being enhanced around 10-fold. Similar to F12PAP-mag2, *trans* and *cis* peptides of this variant showed a difference in membrane-lytic activity (see Materials and Methods, Fig. S1).

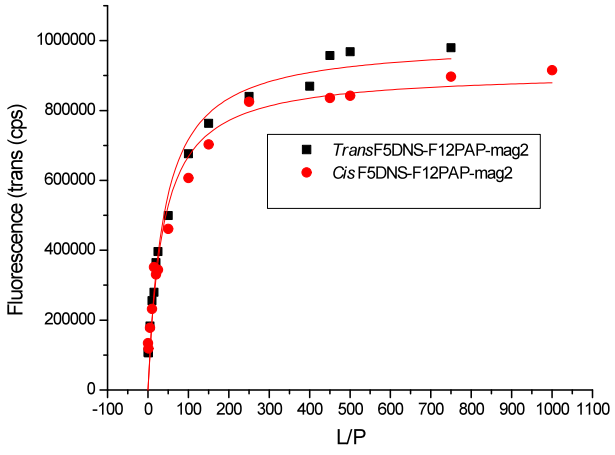

Figure 8. Characterization of binding affinities for F5DNS-F12PAP-mag2. This experiment was performed with 2 μM peptide and varying concentrations of lipids. The graph was plotted with dansyl fluorescence at 502 nm versus L/P ratio. *Trans* F5DNS-F12PAP- mag 2, $K_{D,\,app}$ = 39; *Cis* F5DNS-F12PAP- Mag 2, $K_{D,\,app}$ = 36.

In the binding affinity experiment (Fig. 8), 2 μM peptide and varying concentrations of lipids were used and it turned out that binding affinities were comparable for these two peptide isomers towards LUVs (POPC/POPG 1/1). Additionally, under the leakage assay conditions in Fig. 7 (P/L = 1/250), all peptide molecules were bound for both isomers based on the apparent K_d values, indicating that the binding affinity did not account for the lytic activity difference.

We then characterized the secondary structures of both isomers (Fig. 9) in small unilamellar vesicles (SUVs) made of POPC/ POPG 1/1 with the P/L ratio of 1/250 to make sure an altered secondary structure of the bound peptides was not the cause of the lytic difference. The obtained CD spectra for the *trans* and *cis* isomers of F5DNS-F12PAP-mag2 showed identical α-helix structures, eliminating the possibility that secondary structure propensities afforded the difference in membrane-lytic activity.

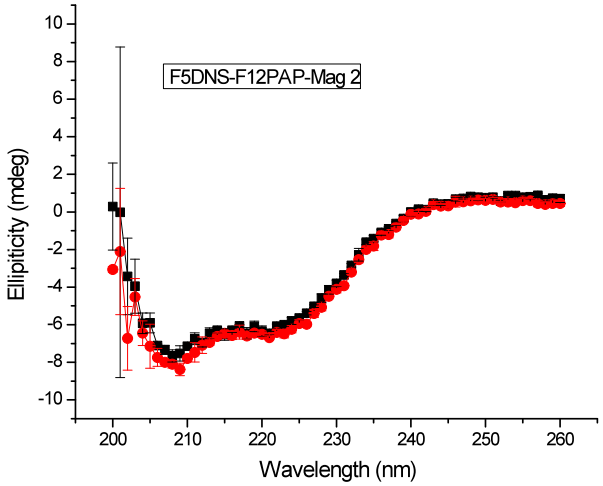

Figure 9. CD spectra of F5DNS-F12PAP-mag2 (peptide concentration 10 μM) in the presence of POPC/POPG 1/1 SUVs (lipid concentration=2.5 mM, P/L = 1/250). Black curve, *trans* isomer; red curve, *cis* isomer.

With both binding affinity and secondary structure excluded, the difference in membrane-lytic activity has to stem from the different peptide membrane-disturbing ability. As mentioned in the introduction (Fig. 1), three mechanisms are related to membrane-disturbing abilities: transient or permanent pore formation or complete membrane disruption.

Dynamic Light Scattering (DLS) measurements were first taken to monitor the integrity of LUVs with peptide addition, and no difference in vesicle size and dispersion implied that the vesicles were intact, eliminating the complete membrane disruption mechanism. Inspired by Matsuzaki's study about mag2[31], we used a fluorescence-quenching method to detect if transient or permanent pores formed under our experimental conditions (see Materials and Methods, Scheme S11). In this experiment, symmetrically NBD-PE labeled LUVs (POPC/POPG/NBD-PE = 1/1/0.005) were incubated at 30 °C with peptides for 2 hr when membrane lysis almost reached the plateau. Dithionite was then added to reduce NBD groups available.

In Matsuzaki's work, inner leaflet NBD-PE labeled LUVs (egg PC/egg PG/NBD-PE = 1/1/0.005) have been used to prove that 12-Trp magainin 2 induced the coupled transbilayer transport ions and lipids by forming a short-lived pore during peptide translocation[33]. If our peptides induce transient pore formation in a similar lipid flip-flop coupled manner, then when leakage reaches the plateau, most of the peptide translocation should deactivate and the pores dissociate, leaving almost no chance for dithionite reduction of NBD groups located in the inner leaflet. If permanent pore form, however, a

---

[33] Matsuzaki, K.; Murase, O.; Fujii, N.; Miyajima, K. Biochemistry, **1996**, *35*, 11361-11368

certain percentage of inner leaflet NBD quenching should be expected because dithionite could enter the inside through the pores.

Two control experiments were done to validate this method. Firstly, addition of dithionite into the LUVs with no peptides resulted in complete fluorescence quenching of NBD groups on the outer leaflet (0% quenching of NBD groups in the inner leaflet), while dithionite addition into the LUVs incubated with 0.1% Triton X-100 resulted in complete quenching of all NBD groups (100% quenching of NBD groups in the inner leaflet).

From Fig. 10, we could tell that at low peptide concentration (2 μM), no permanent pores formed and only the fluorescence of NBD groups in the outer leaflet was quenched; while at concentrations as high as 9 μM, stable pores formed and complete NBD fluorescence quenching occurred (F5W-F12PAP-mag2 has similar properties as F5DNS-F12PAP-mag2).

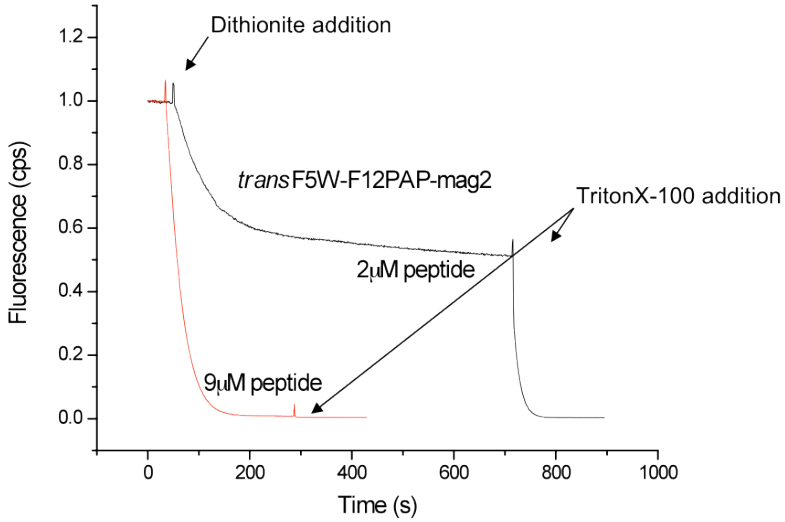

Figure 10. NBD fluorescence-quenching assay with *trans* F5W-F12PAP-mag2. 1 mM POPC/POPG 1/1 LUVs (symmetrically labeled with 0.25% NBD-PE) were incubated with 2 and 9 μM peptides at 30 °C. Dithionite was added 2 hr later (final concentration 10 mM), and addition of 10% Triton X made all NBD lipids accessible to dithionite

A distinctive feature of transient pore formation is peptide translocation. It is highly likely that the *trans* peptide induces a higher percentage of peptide translocation coupled with a larger percentage of Tb^{3+} leakage. To prove this hyphothesis, a modified enzyme digestion method was adopted to measure the fraction of peptide translocated[31] (scheme 1).

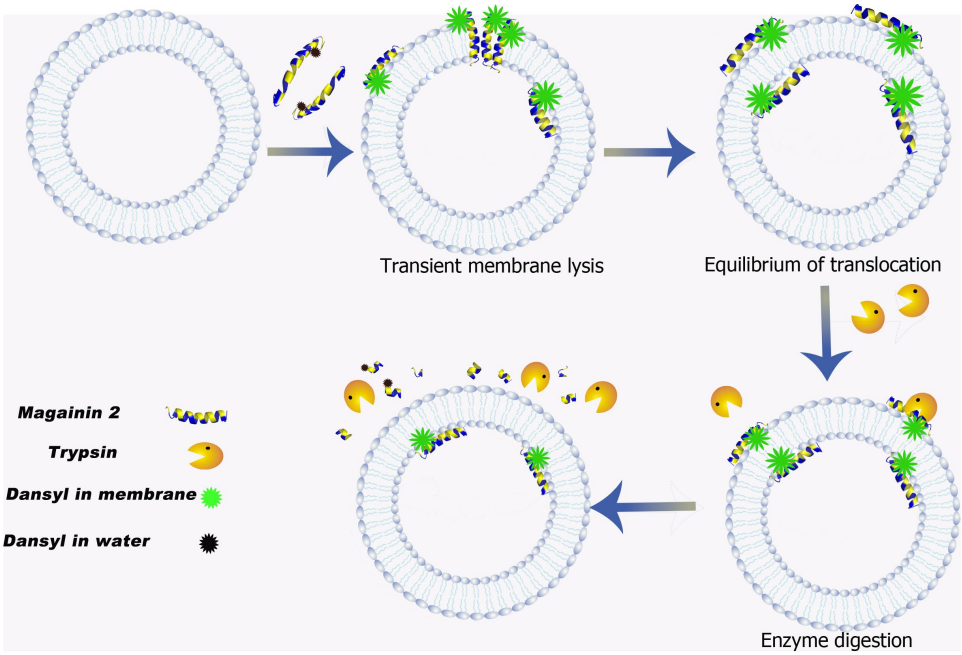

Scheme 1. Enzyme digestion assay

Trypsin is an enzyme that effectively hydrolyzes mag2. F5DNS-F12PAP-mag2 and the LUVs (POPC/POPG/NBD-PE = 1/1/0.005) were used in this method. Addition of this peptide into the LUVs resulted in rapid binding of the peptide to the membrane and enhanced fluorescence intensity of dansyl group F_m. After 2 hrs incubation, trypsin was added to selectively digest the peptide molecules located in the outer monolayer while leaving the translocated peptides intact. The digested peptide fragments were

desorbed from the membrane back into the buffer, leading to a decrease in fluorescence intensity of dansyl. The resulting fluorescence intensity F_t was a mixture of fluorescence intensity from peptide translocated and digested peptide in the solution. Incubation of peptides with trypsin first followed by LUVs addition afforded complete digestion of peptide molecules by trypsin and no binding to the membrane, which created F_w. Based on F_w, F_m, F_t, we were able to calculate the percentage as well as amount of peptide translocated for both isomers (Fig. 11).

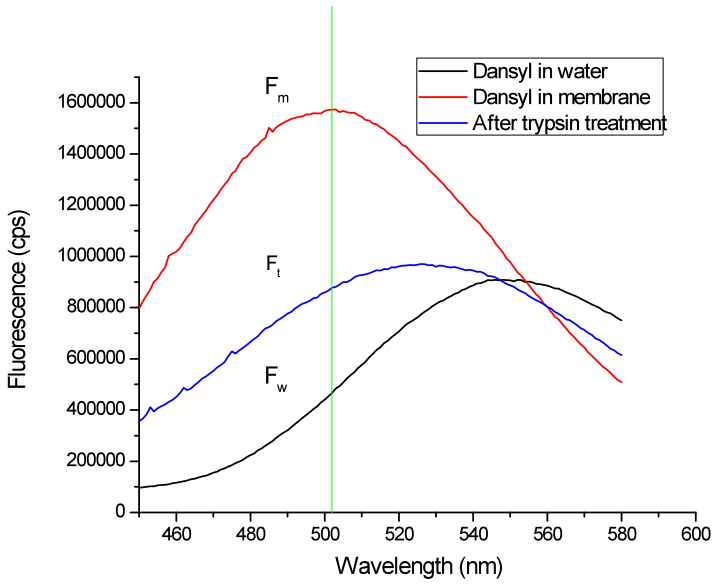

Figure 11. Calculation of percentage of peptide translocation

	1 μM *trans*+500 μM lipids	1 μM *cis*+500 μM lipids
Percentage of translocation	33%	7%
Percentage of leakage	32%	9%

Table 1. Peptide translocation measured by enzyme digestion assay. For each experiment, 1 μM peptide was incubated with 0.5 mM LUVs at room temperature for 2 hrs, followed by trypsin treatment. Dansyl fluorescence was recorded before and after trypsin treatment, respectively. Data presented here are the average of duplicated samples

Data in Table 1 shows that under the same conditions, the *trans*-peptide induced a larger fraction of Tb^{3+} leakage as well as a higher percentage of peptide translocation than the *cis*-isomer did.

Based on these results, we concluded that with same amount of bound peptides and similar secondary structures, the *trans*-peptide not only elicits a higher potency in membrane lysis compared with the *cis*-peptide, but also a higher degree of peptide translocation when P/L is lower than the threshold P/L^* (we didn't measure the exact value of P/L^*, but it is very likely that the *trans* peptide has a much lower P/L^* than the *cis* peptide does). By looking at the azobenzene structure, it is conceivable that the different membrane-lytic activity is due to the huge conformational difference between the two azobenzene isomers, and to be more specific, length difference. For *trans* azobenzne, the distance between two para carbons is 9.2 Å, while for *cis* azobenzene it decreases to 5.4 Å. To test this hypothesis, we designed a series of mag2 variants carrying side chains with varying length at the same position of azobenzene and all labeled with a dansyl group. These side chains are phenyl, biphenyl, and terphenyl with the distance between two para carbons being 2.8 Å, 7.2 Å, and 11.6 Å respectively (Fig. 12, unnatural amino acid Fmoc-biphenyl-OH and Fmoc-terphenyl-OH were used). Binding affinities were characterized by the same method (Fig. 13a) and a leakage assay was carried out under conditions where all peptide molecules were bound to the membrane for all variants (Fig. 13b).

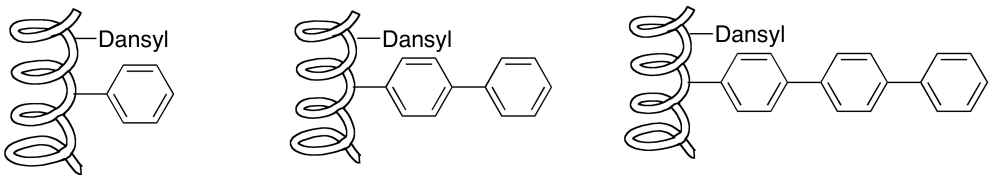

Figure 12. Structures of F5DNS-mag2, F5DNS-F12biphenyl-mag2 and F5DNS-F12terphenyl-mag2.

The diverse binding affinities can be attributed to the different hydrophobicities of the three side chains, while L/P ratio of 500/1 for the leakage assay guaranteed all peptide molecules were completely bound to the membrane for these variants. Thus it is reasonable to conclude that the observed difference in membrane lysis is due to the different in side chain length. With the longest side chain, F5DNS-F12terphenyl-mag2 showed the highest potency and F5DNS-mag2 showed the lowest. This result confirmed our hypothesis that the side chain length plays a major role in determining the membrane-lytic activity of mag2. Moreover, the membrane-lytic activities were measured under varied peptide concentrations against 500 μM LUVs (POPC/POPG 1/1) and an EC_{50} obtained was 3.44 ± 0.06 μM, 1.37 ± 0.02 μM and 1.11 ± 0.02 μM for F5DNS-mag2, F5DNS-F12biphenyl-mag2 and F5DNS-F12terphenyl-mag2 respectively (see Materials and Methods, Fig. S2)

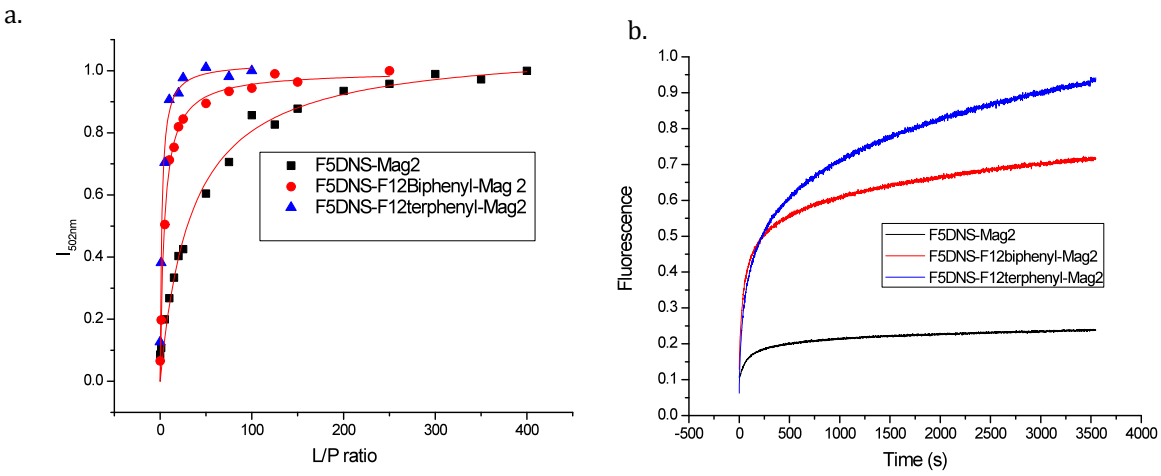

Figure 13. Characterization of binding affinities and lytic activity of three mag2 mutants. a.) Binding affinity experiment was performed with 2 μM peptide and varying concentrations of lipids. The graph was plotted with dansyl fluorescence at 502 nm versus L/P ratio. F5DNS-mag2, $K_{D, app}$ = 35; F5DNS-F12biphenyl-mag2, $K_{D, app}$ = 5; F5DNS-F12terphenyl-mag2, $K_{D, app}$ = 2. b.) Three peptide mutants show increasing extent of membrane lysis with increased side chain length. This leakage assay was performed with 1 μM peptide and 500 μM LUVs made of POPC/ POPG 1/1 at room temperature under stirring. Data presented are the average of three measurements (standard deviations as absolute percentage were less than 8%)

To elucidate this phenomenon, it is important to introduce 'interfacial activity'[34] into our system. Interfacial activity is described as the ability of a molecule to bind to a membrane, partition into the membrane-water interface, and to alter the packing and organization of the lipids. When mag2 binds to the lipid bilayers, the hydrophobic region, mainly consisted of aromatic residues (phenyl, biphenyl and terphenyl), drives a deep perturbation into the lipid bilayers, and the nearby polar residues such as lysine promote the incursion of lipid polar groups deeper into the membrane, along with the polar residues of mag2. A more extended hydrophobic side chain would be able to perturb the membrane to a higher degree, due to a strengthened interaction between the hydrophobic

[34] Wimley, W.C. *ACS Chem. Biol*. **2010**, *5*, 905-917

side chains and neighbor hydrophobic moieties. The extent of perturbation is coupled with peptide translocation and membrane-lytic activity as well. Here we propose the importance of side chain length in determining membrane lysis activity, which may shed light on design and engineering membrane-active peptides. However, there is still difficulty in rational and systematic engineering of such peptides because 'interfacial activity' is an integrated effect of peptide's amphipathicity, balance between hydrophobic and polar residues, the potential to alter the packing and curvature of lipids.

2.2.3 Conclusions

In summary, we have incorporated a photolabile side chain into antimicrobial peptide mag2 and demonstrated photo-switchable membrane-lytic activity of this peptide. Unlike traditional modifications of binding affinity and secondary structure of the antimicrobial peptide, *trans-cis* isomerization alters peptide 'interfacial activity' coupled with membrane-lytic activity, upon which we could manipulate the peptide activity easily with light irradiation. In addition to that, our mechanistic study suggests that side chain length plays an important role in interfacial activity, while more studies are needed to gain a better understanding of it and direct rational design of membrane-active peptides.

Finally, the incomplete photo-conversion of azobenzene between *cis* and *trans* isomers sets intrinsic limits on the degree of photomodulation of AMPs activity. By using other azobenzene derivatives that undergo high conversion from the t*rans* to the *cis* isomer, we may be able to realize the complete "switch on and off" strategy. Moreover, it is more beneficial if we could create a long-wavelength irradiation located in the

biological transparent spectral range (800-1000nm) with the capability of penetrating more deeply into the biological tissues.

2.3 Enhancement of selective toxicity by environment-responsive residues

2.3.1 Background and experimental design

People have utilized environment-responsive residues in development of pH-sensitive membrane-active peptides. Our group has successfully developed a 'smart' mag2 functionalized with tetrafluorotyrosine (f_4Y) as effective pH sensor[35]. Three Phe residues at the hydrophobic face were replaced by f_4Y, and because pKa of f_4Y is 5.6, when the pH dropped from 7.0 to 5.0, the membrane-lytic activity of the mag2 variant went through a dramatic increase. Here, pH was employed as the external stimuli to activate mag2.

With the continuous effort in exploring the applications of environment-responsive residues in AMPs, we tried to develop another 'smart' peptide that could only be activated upon contact with the negatively charged membrane. Fmoc-LHA-OH is an unnatural amino acid developed by our group with an environment-responsive LHA moiety (Fig. 14). The pKa of LHA is around 8 in aqueous solution (protonated-positively charged), and expected to be downshifted in a hydrophobic environment (deprotonated-neutral). Replacement of 1-3 Phe residues in the hydrophobic face of mag2 with LHA group would strengthen the electrostatic interactions between mag2 and negatively

[35] Wang, F.; Qin, L.; Wong, P.; Gao, J. *Org. Lett.* **2010**, *13*, 236-239

charged membrane due to the increased overall positive charge at pH 7, while it would decrease or even wipe out the binding of mag2 to neutral membranes because of decreased hydrophobic interactions. Thus the difference in binding affinities is amplified. Furthermore, once LHA-incorporated mag2 is bound to negatively charged membrane, LHA should be deprotonated in the hydrophobic environment and the membrane-lytic activity of mag2 should be restored. In summary, the selectivity of LHA incorporated mag2 variants would be enhanced due to the largely decreased or lost binding to neutral membrane, and the activity of mag2 could only be turned on when binding to negatively charge membrane.

However, according to the measured pKa values of LHA moiety (Fig. 14, pKa measurement see Materials and Methods, Fig. S4, S5), different membranes (neutral, positive, and negative) influenced the pKa values quite differently. This was also observed in a published work measuring pKa of fluorescent pH indicators in different membranes[36]. The measured pKa of LHA moiety was around 8.2 in aqueous solution, 6.5 in neutral membrane and 8.4 in negatively charged membrane.

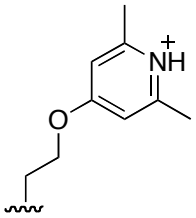

Environment	pKa
Water	8.2
DPC micelles (Neutral)	6.5
SDS micelles (Negatively charged)	8.4

Figure 14. pKa change of LHA in different environment

[36] Fernandez, M.S.; Fromherz, P. *The Journal of Physical Chemistry*, **1977**, *81*

Thus the major concern of this strategy lies in the fact that negatively charged membrane increases the pKa to such a large extent, and LHA would remain positively charged on negatively charged membranes, the membrane-lytic activity of the bound peptide could be sacrificed because of the broken amphiphathicity. Still, we were curious to find out if the enlarged binding affinity difference could result in enhanced selectivity at the price of possible activity loss.

2.3.2 Results and Discussion

Two mag2 variants were prepared: The single LHA substituted variant N-DNS-F12LHA-mag2a and triple mutant N-DNS-TriLHA-mag2. Another peptide N-DNS-mag2a was synthesized as a control. The binding affinities were evaluated based on dansyl fluorescence.

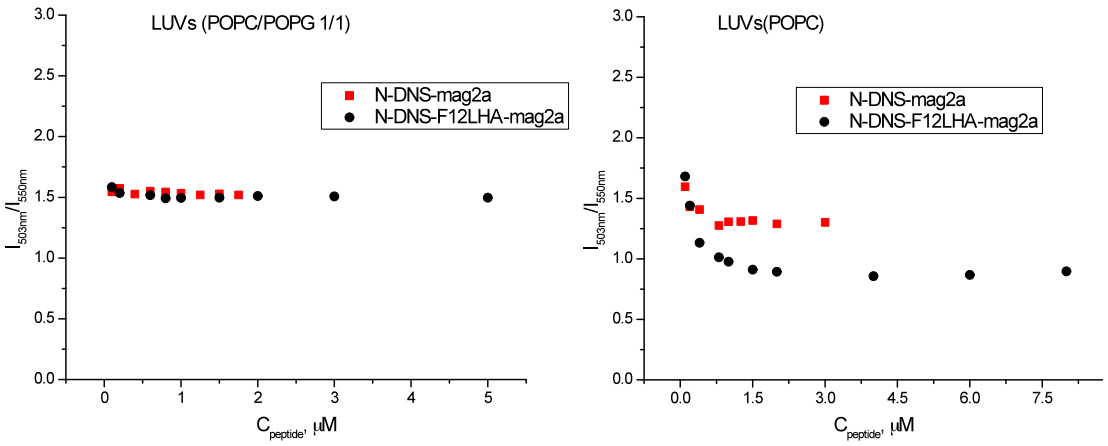

Figure 15. Characterizationi of N-DNS-mag2a and N-DNS-F12LHA-mag2a binding affinities. This experiment was performed with 100 μM LUVs (POPC and POPC/POPG 1/1) and varying concentrations of peptides. The graph was plotted with dansyl fluorescence I_{502nm}/I_{550nm} versus peptide concentration.

In Fig. 15 for negatively charged LUVs (POPC/POPG 1/1), the binding affinities were comparable between these two peptides, however for neutral LUVs (POPC), binding affinity of the single LHA mutant was largely decreased because of loss of hydrophobic interactions. Membrane-lytic activities were measured under varied peptide concentrations and EC_{50} was obtained for comparison. EC_{50} of the LHA single mutant was 2-fold higher than the control (N-DNS-mag2a) on the negatively charged membrane, and for neutral membrane, EC_{50} increased 4-fold, leading to a selectivity enhancement about 2-fold. There was moderate enhancement in cell-based assays, as shown in table 2.

Peptide	EC_{50} (μM)		MIC (μg/ml)	HC_{50} (μg/ml)
	POPC LUVs	POPC/POPG 1/1 LUVs		
N-DNS-mag2a	1.10±0.02	0.51±0.02	4	43
N-DNS-F12LHA-mag2a	4.68±0.20	1.00±0.01	16	215
N-DNS-TriLHA-mag2a	Inactive	Limited activity	N/A	N/A

Table 2 Membrane-lytic, Antimicrobial and Hemolytic activities of LHA incorporated mag2. For membrane-lytic activity measurement, 0.1 mM LUVs were used for each experiment.

For the triple mutant, there was almost no binding to neutral membrane (the maximum dansyl fluorescence peak stayed at 550 nm and no shift was observed). Out of our expectation, binding to negatively charged membrane was also very limited (Fig. 16). Moreover, limited membrane-lytic activity was observed for both LUVs (POPC/POPG 1/1) and LUVs (POPC).

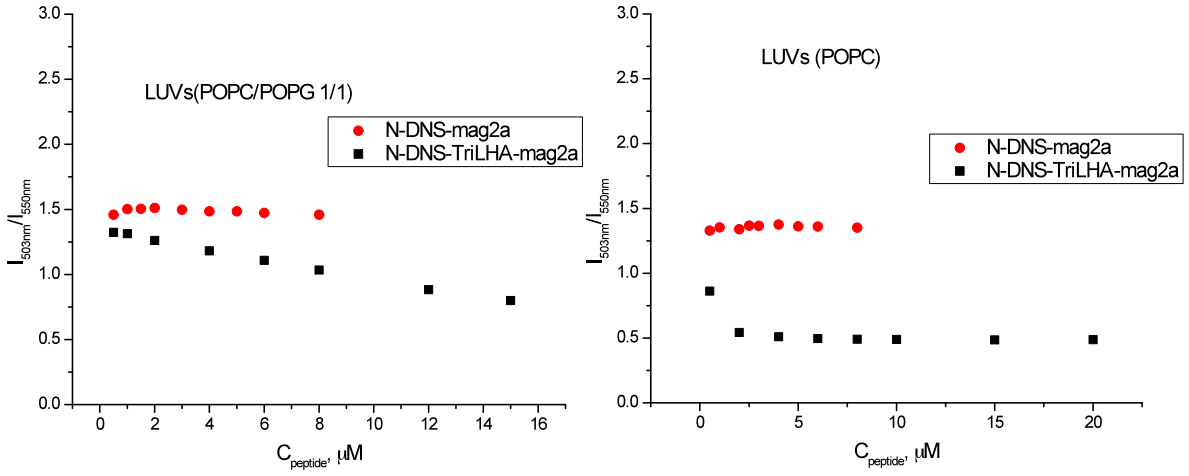

Figure 16. Characterizationi of N-DNS-mag2a and N-DNS-TriLHA-mag2a binding affinities. This experiment was performed with 100 μM LUVs (POPC and POPC/POPG 1/1) and varying concentrations of peptides. The graph was plotted with dansyl fluorescence I_{502nm}/I_{550nm} versus peptide concentration.

Based on our previous concern, it is conceivable that these LHA incorporated mag2 have lost part of the ability to fold into active α–helix after binding. CD experiments were then conducted to address this question.

From CD measurements, all three peptides were able to fold into α–helices in PBS buffer with 50% TFE at both pH 7 and 9, indicating that the protonated and deprotonated LHA side chain caused no difference in the ability of mag2 folding.

For the single variant, it had similar binding affinity and α helicity on POPC/PCPG 1/1 membrane as the control peptide N-DNS-mag2a , however, EC_{50} was 2-fold higher. The protonated LHA in the bound single mutant, compared to Phe in the control peptide, may disturb the interfacial activity of mag2 by placing a postively charged residue in the hydrophobic face.

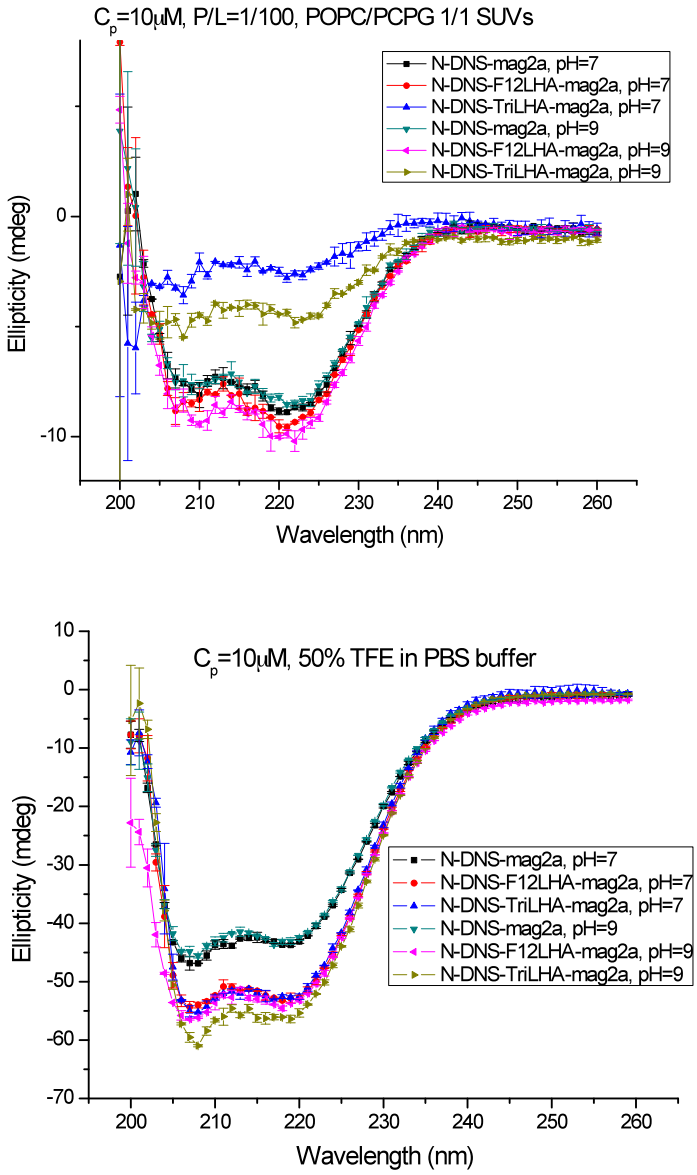

Figure 17. CD measurements of three mag2 variant in both SUVs (POPC/POPG 1/1) and 50% TFE in PBS buffer

Given the slightly enhanced selectivity of the single variant (2-fold), the effect from enlarged binding affinity difference between neutral and negatively charged

membrane is probably counteracted by the decreased membrane-disturbing ability of bound peptide on negatviely charged membrane. Moreover, since the measured pKa in neutral membrane is 6.5, then the bound peptide on neutral membrane may be more potent (LHA deprotonated) than the bound peptide with positively charged LHA on negatviely charged membrane. This modification has an adverse effect on improving selectivity.

In SUVs (POPC/PCPG 1/1), the triple variant was mostly random coil at pH 7 and showed moderately improved α helicity at pH 9. The main reason for the secondary structure loss at pH 7 was due to the poor binding to the negatively charged membrane and most of the peptide molecules remained in the aqeous solution. Compared to the single variant, it is even harder for the triple variant to fold into α-helix with three positively charged residues on the hydrophobic face. The strong electrostatic interactions between positively charged LHA and negatively charged lipids may prevent the peptides from folding into correct α-helix. And this may explain why the triple variant has even lower binding affinity to negatively charged membrane than the single mutant does: the bound triple mutant peptides are unstructured on membrane and cover a larger surface than structured mag2 α-helix, leaving less space for more peptide to bind; the triple mutant has three more positive charges per peptide molecule than mag2 and the electrostatic interaction is saturated rapidly.

2.3.3 Conclusions

To conclude, we observed a small enhancement in selectivity (2-fold) by functionalizing mag2 with an environment-responsive LHA moiety. It is exciting to see a single amino acid replacement at the hydrophobic face has a significant impact on peptide binding to neutral membranes. However, we underestimated the effect of different charged membranes on the pKa of the environment-responsive moiety and the following influence on peptide membrane-disturbing ability. It would be interesting to see if the triple mutant could fold into an α helix and induce membrane lysis with the help of a preinstalled secondary structure stabilizer.

2.4 Side-chain staple facilitates on-membrane action of magainin 2

2.4.1 Background and experimental design

Stabilization of peptide α-helical structures via side-chain stapling has been successfully utilized in studies of protein-biomacromolecule interactions[37,38]. In the past decade, one of the most popular methods of helix stabilization has been the use of ring-closing metathesis (RCM) to link the side chains at *i* and *i*+4 or *i*+7 positions[39]. Installation of the all-carbon cross-linking has been shown to increase both helical contents and peptide binding affinity, also remarkably decrease the rate of proteolysis. In addition to peptide cyclization through RCM, the use of the Huisgen Cu (I) catalyzed 1,3-

---

[37] Walensky, L.D.; Kung, A.L.; Escher, I.; Malia, T.J.; Barbuto, S.; Wright, R.D.; Wagner, G.; Verdine7, G.L.; Korsmeyer, S.J. *Science* **2004**, *305*, 1466-1470.

[38] Kajino, M.; Fujimoto, K.; Inouye, M. *J.Am.Chem.Soc.* **2011**, *133*, 656-659

[39] Schafmeister, C.E.; Po, J.; Verdine, G.L. *J. Am. Chem. Soc.* **2000**, *122*, 5891

dipolar cycloaddition reaction has been reported[40,41]. This click reaction is simple, mild and has high yields. Inspired by these accomplishments, we hypothesized that a side-chain staple may also improve the interaction between mag2 and membranes because of the pre-organized secondary structures in aqueous solution, and even this side-chain stabilization could affect peptide on-membrane activity as well.

Besides, a side-chain staple might be a convenient tool for us to manipulate the membrane-lytic activity of AMPs by providing a pre-organized scaffold. For example, for the second project a side-chain staple may help the triple LHA mutant recover certain ability to fold into correct α helical structure; for the 'interfacial activity' study, we could study the most relevant factors towards optimization of 'interfacial activity' by systematically change the numbers, positions and arrangements of hydrophobic and polar residues on the basis of a strong pre-stabilized secondary structure, without worrying about these manipulations may disrupt the folding abilities a lot.

2.4.2 Results and Discussion

Considering the reported insolubility of peptides with a hydrophobic staple generated by RCM and expensive, toxic ruthenium based catalysts involved[42], we chose the triazole stapling approach. To construct stapled mag2, we placed synthetic azide and alkyne modified amino acid at certain positions separately, and the triazole staple

---

40 Le Chevalier Isaad, A.; Papini, A. M.; Chorev, M.; Rovero, P. *J. Pept. Sci.* **2009**, *15*, 451.

41 Cantel, S.; Halperin, J.A.; Chorev, M.; Scrima, M.; D'Ursi, A.M.; Levy, J.J.; DiMarchi, R.D.; Le Chevalier, A.; Rovero, P.; Papini, A.M. *Adv. Exp. Med. Biol.* **2009**, *611*, 175.

42 Kawamoto, S.A. A dissertation submitted in partial fulfillment of the requirements for the degree of Doctor of Philosophy (Medicinal Chemistry) in The University of Michigan 2010

spanning the *i*, *i*+4 positions was generated by click reaction (Fig. 18). Two variants were synthesized, each containing a distinctively localized cross-link (Fig. 18). A dansyl group was incorporated at the N-terminal of all peptides to evaluate binding abilities and C-terminal amide was introduced to keep the total charge unchanged. For mag2a-1 and mag2a-1S, E19 was replaced with A to maintain the overall positive charge since K11 was mutated to azide modified unnatural amino acid.

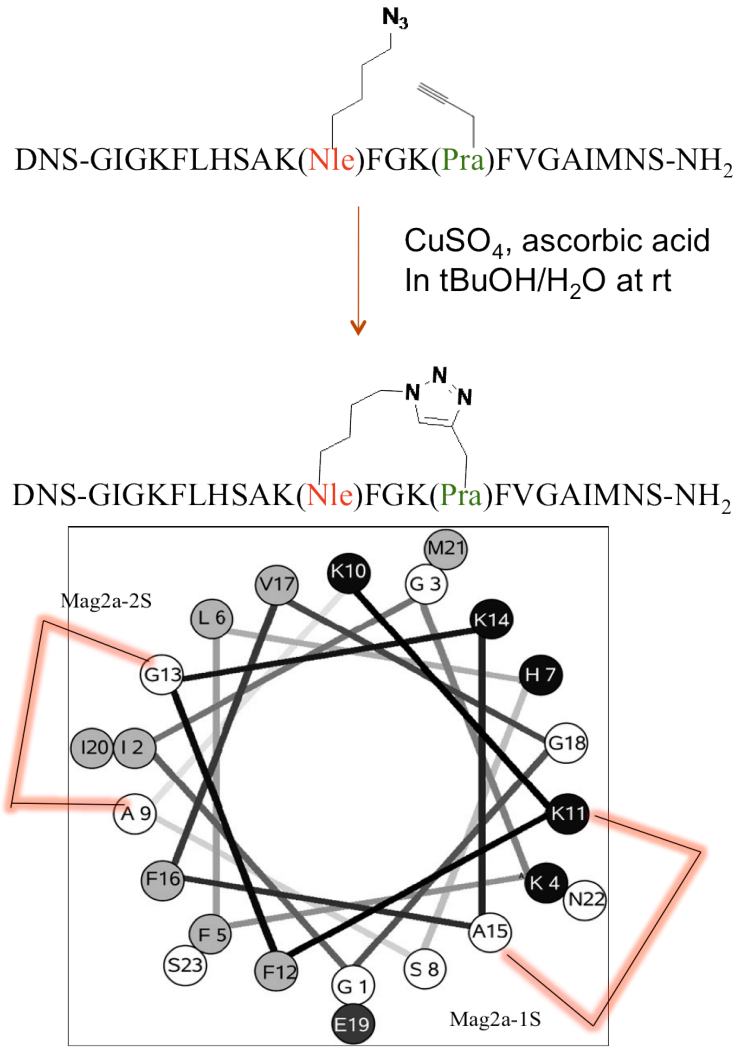

Figure 18. Scheme of cyclization and two mag2 variants with a triazole staple at different position

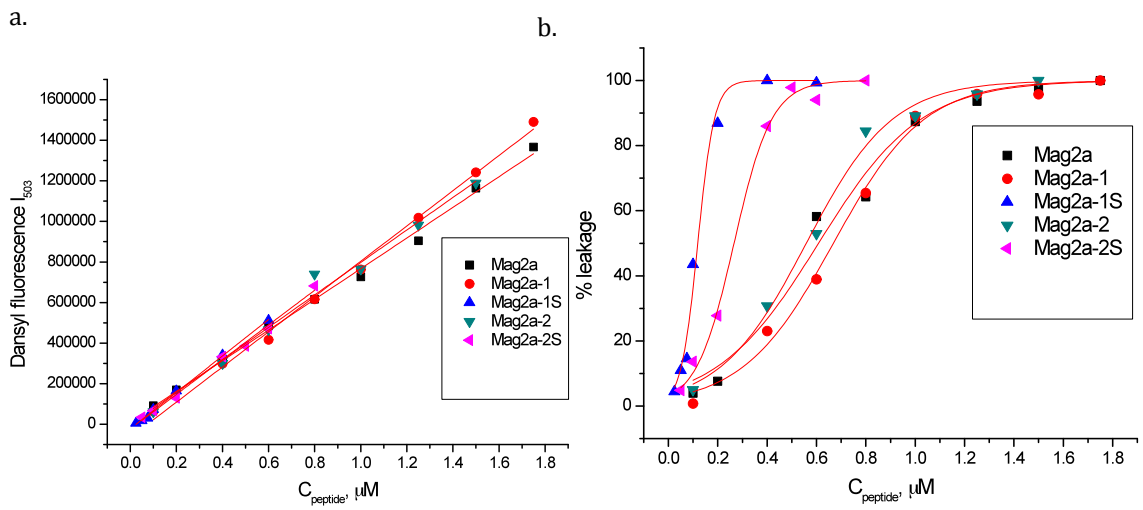

Figure 19. Binding affinities and Lytic activities of linear and stapled mag2 against LUVs (POPC/POPG 1/1). (a) Dansyl fluorescence at 503 nm under the same condition. (b) Leakage of 100 μM LUVs incubated with varying concentrations of peptides from 25 nM to 1.75 μM at 30 °C for 2 hrs

Binding affinities of peptide mutants were examined first based on dansyl fluorescence (Fig. 19a). For each peptide variant, the intensity at 503 nm is plotted versus peptide concentration. The similar intensity for each peptide at certain concentration indicated that all peptides have similar binding affinities.

To evaluate the structural impact of installing a triazole staple into mag2, we conducted circular dichroism (CD) in PBS buffer as well as in SUVs (POPC/POPG 1/1) (Fig. 20). Mag2a and mag2a-1 were unstructured in aqueous solution as expected, while mag2a-2 was helical. It is conceivable that mag2a-2 forms a helical bundle in aqueous solution given its largest hydrophobicity, which affords increased hydrophobic interaction between peptide α-helices (Hydrophobicities of the peptides were evaluated

based on their retention times on reversed phase HPLC[43,44], table 3). A similar phenomenon was observed when fluorinated amino acids were incorporated into mag2, only the most hydrophobic mutant was significantly helical in aqueous solution. It turned out that stable helical bundles were formed, resulting in the lowest antimicrobial activity[45]. In PBS buffer, mag2a-1S showed significantly enhanced helicity compared to corresponding linear peptide mag2a-1, and mag2a-2S showed moderate improvement compared to mag2a-2. In SUVs solutions, mag2a-1S maintained the helicity enhancement over mag2a-1, however mag2a-2S had similar helicity with mag2a-2. Noticeably, all the CD measurements with membrane were done under the conditions (L/P 250/1) that all peptides were bound, thus the difference in helicity was exclusively caused by side-chain stapling effect.

Table 3: Hydrophobicities and α helicities of linear and stapled mag2

Peptide	Sequence *=Nle, *=Pra	t_R[a] (min)	α helicity[b]	
			PBS	SUVs
Mag2a	DNS-GIGKFLHSAKKFGKAFVGEIMNS-NH_2	18.7	6%	60%
Mag2a-1 (linear)	DNS-GIGKFLHSAK*FGK*FVGQIMNS-NH_2	20.5	9%	66%
Mag2a-1S (cross-linked)	DNS-GIGKFLHSAK*FGK*FVGQIMNS-NH_2	24.2	17%	85%
Mag2a-2 (linear)	DNS-GIGKFLHS*KKF*KAFVGEIMNS-NH_2	25.8	20%	75%
Mag2a-2S (cross-linked)	DNS-GIGKFLHS*KKF*KAFVGEIMNS-NH_2	23.5	20%	75%

[a]Retention times were determined by phase reversed HPLC. [b]Values obtained from circular dichroism spectroscopy studies.

43 Tachi,T.; Epand,R.F.; Epand,R.M.; Matsuzaki,K. *Biochemistry*, **2002**, *41*, 10723-10731.

44 Niemz, A.; Tirrell, D.A. *J.Am.Chem.Soc.* **2001**, *123*, 7407-7413

45 Meng, H.; Kumar, K. *J. Am. Chem. Soc.* **2007**, *129*, 15615-15622

a.

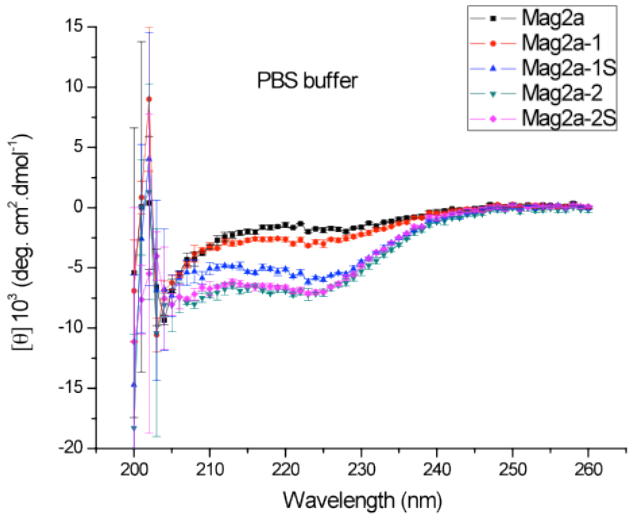

b.

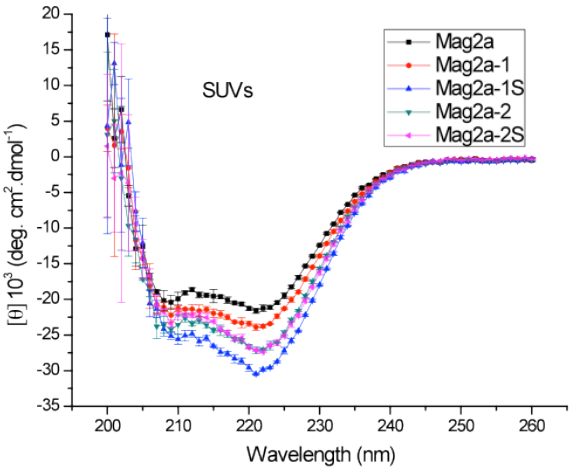

Figure 20. Secondary structures of linear and stapled mag2. Circular dichroism spectra of (a) mag2a, mag2a-1, mag2a-1S, mag2a-2, mag2a-2S in PBS buffer, (b) 10 μM peptide incubated with 2.5 mM SUVs (POPC/ POPG 1/1).

The membrane-lytic activities of these mag2 variants were then evaluated by Tb^{3+}/DPA membrane leakage assay (Fig. 19b). EC_{50} was determined for each peptide

variant (table 4). Two linear precursors had similar membrane-lytic activities relative to the parent peptide mag2a, while two stapled peptides had increased activities, with improvements in EC_{50} values from 2 folds to almost 7 folds. At concentration as low as 0.1 μM, the most potent variant mag2a-2S caused almost full leakage while mag2a and two linear precursors were not active at all. The trend of EC_{50} corresponded very well with the α helicities of these peptides on membrane, though with similar α helicities, mag2a-2S is 2-fold more active than mag2a-2.

Table 4: EC_{50} and PC_{50} of the linear and stapled mag2

Peptide	EC_{50}[a] (μM)	PC_{50}[b] (μM)
Mag2a	0.61 ± 0.03	0.64 ± 0.02
Mag2a-1 (linear)	0.67 ± 0.01	0.61 ± 0.03
Mag2a-1S (cross-linked)	0.11 ± 0.01	0.17 ± 0.01
Mag2a-2 (linear)	0.56 ± 0.02	0.56 ± 0.03
Mag2a-2S (cross-linked)	0.27 ± 0.01	0.31 ± 0.01

[a]The EC_{50} values were extracted by extrapolation of the fitted curve to 50% lysis of POPC/POPG 1/1 LUVs. [b]The PC_{50} values were extracted by extrapolation of the fitted curve to 50% permanent pore formation of POPC/POPG 1/1 LUVs.

Since we did not observe any difference in binding abilities, the increased membrane-lytic activity of stapled mag2 could only result from the increased membrane-disturbing activities of the bound peptides.

To characterize the effect of side-chain stapling on membrane disturbing ability, first of all, DLS was used to monitor the integrity of liposome going through the

membrane lysis, and no difference in vesicle size and dispersion implied that liposome vesicles were intact. Then we tested this set of mag2 variants with the same NBD fluorescence-quenching experiments used for photoswitchable mag2 variants to observe transient or permanent pore formation. This time the experiment was conducted under varied peptide concentrations.

Surprisingly, we observed permanent pores formation with all our peptide variants through this method. With dithionite addition, different extents of inner leaflet NBD groups quenching were observed for samples with different peptide concentrations. Then transient pore formation could be excluded because NBD groups in the inner leaflet were only available for dithionite reduction with stable pores formed on the membrane. Thus the percentage of NBD groups quenched in the inner leaflet reflected the percentage of LUVs with stable pores on the membrane. If we plotted this value versus peptide concentration, we obtained PC_{50} for each peptide (Fig. 21). Perfect correlation between pores formation curve and membrane leakage curve indicated that membrane lysis is directly coupled with stable pores formation (Fig. 19b and Fig. 21). Therefore different lytic activity of mag2 variants actually came from different permanent pore formation abilities of the bound peptide molecules.

Previous studies of H. Huang indicate stable pore formation only occurs when P/L reaches a threshold *P/L**[46,47]. For AMPs they have studied (alamethicin, melittin, magainin and protegrin), the threshold concentration *P/L** varies from 1/200 to ~1/10

---

[46] Ludtke,S.J.; He,K.; Heller,W.T.; Harroun,T.A.; Yang,L.; Huang,H.W. *Biochemistry*, **1996**, *35*, 13723-13728.

[47] Huang,H.W. *Biochim.Biophys.Acta*, **2006**, *1758*, 1292-1302

(P/L~1/200 is the detectable limit of their experimental methods). Under our experimental conditions, the observed permanent pores formation at low P/L ratio of 1/2000 for this set of mag2 variants indicates that the values of *P/L** are significantly lowered down.

Though our experimental results do not lead to a detailed structural description of these stable pores, we have proved that the increased α-helicity of mag2 in aqueous solutions as well as on membrane actually facilitates stable pore formation. Previous studies concerning the role of helicity in the antimicrobial effects utilized D-amino acid substitution to disturb helix formation. A systematic exchange of two neighboring residues in magainin by their D-enatiomers resulted in decreased helicity in the membrane-bound state and distinctly reduced its permeabilizing activity against neutral (POPC) and moderately negatively charged membrane (POPC/POPG 3/1)[48, 49]. Investigation with a cationic amphipathic KLAL model peptide confirmed that the enhanced membrane disturbing ability is related to the size of the hydrophobic helix domain determined by the peptide helicity[50].

It is conceivable that a pre-organized α-helix in aqueous solution may help peptide to bind to membrane more easily. However, for mag2a, the measured apparent K_d is as high as 6 already (see Materials and Methods, Fig. S3), the enhancement might be undetectable under our experimental conditions, and it is not surprising that we didn't

---

48 Dathe,M.; Wieprecht,T. *Biochim. Biophys. Acta*, **1999**, *1462*, 71-87.

49 Wieprecht,T.; Dathe,M.; Schumann,M.; Krause,E.; Beyermann,M.; Bienert,M. *Biochemistry,* **1996**, *35*,10844-10853

50 Dathe,M.; Schumann,M.; Wieprecht,T.; Winkler,A.; Beyermann,M.; Krause,E.; Matsuzaki,K.; Murase,O.; Bienert,M. *Biochemistry*, **1996**, *35*, 12612-12622

observe further improvement with side chain staple. For membrane permeabilization, a stabilized and rigidified α-helix on membrane may favor peptide insertion, intermolecular interaction, and further pore stabilization in the similar manner as discussed above.

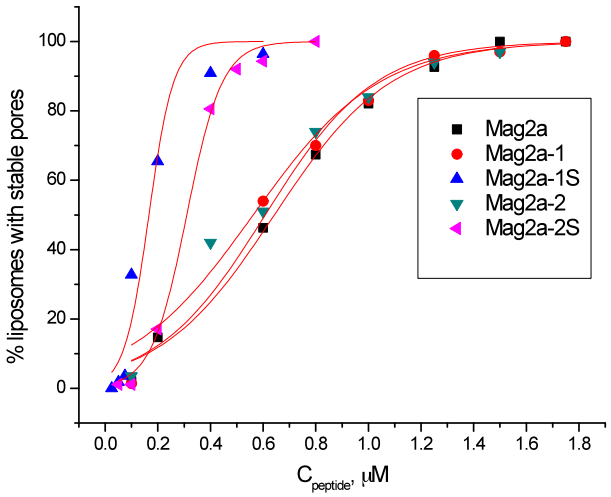

Figure 21. Permanent pores formation of mag2 against POPC/POPG 1/1 LUVs. 100 μM LUVs incubated with varying concentrations of peptides from 25 nM to 1.75 μM at 30 °C for 2 hrs, and dithionite was added (final concentration 10 mM). Fluorescence at 530 nm was monitored until the decrease reached the plateau and the ending point was used for calculation.

With a closer look at the HC_{50} and PC_{50} for each peptide (table 4), we found out the enhancement of activity for mag2a-2S over mag2a-2 is only 2-fold compared to 7-fold difference between mag2a-1S and mag2a-1. Because the triazole group is relatively hydrophilic, for mag2a-1S, the staple is accommodated well on the hydrophilic face, while for mag2a-2S this hydrophilic staple may not be preferred on the hydrophobic face.

Antimicrobial activity and hemolytic activity were tested for each peptide variant. The antimicrobial activity was assessed as a minimal inhibitory concentration (MIC) using turbidity assays against both Gram-negative (*E. Coli*) and Gram-positive (*B.*

subtilis) bacteria (Table 5). All other peptide variants had better or similar antimicrobial activities compared to mag2a with the exception of mag2a-1. Given that the most active members of the antimicrobial host defense peptides have MICs in the range 1~3 μM[51,52], our peptides are already working at the potency limit, thus it is not surprising stapled mag2a show the same efficacy. Mag2a-1 was 16- and 2-fold less active against *E. Coli* and *B. subtilis* compared to other mag2 peptides. A pair of charged residues has been eliminated from mag2a-1, which may impede the diffusion of peptides into bacteria. On the other respect, mag2a-1S was 16- and 2-fold more active than mag2a-1 even with the same sequence, suggesting that stapling may also work for microorganism as well as artificial liposome system.

Table 5: Antimicrobial and Hemolytic Activities of the Peptides

Peptide	MIC[a] (μg/ml)		HC_{50}[b] (μg/ml)
	E. Coli	*B. subtilis*	
Mag2a	4	4	43
Mag2a-1 (linear)	64	8	18
Mag2a-1S (cross-linked)	4	4	12
Mag2a-2 (linear)	4	4	N/D
Mag2a-2S (cross-linked)	4	2-4	N/D

[a]MICs represent at least two independent experiments, each in duplicate, and are reported as the highest determined values. [b]The HC_{50} values were extracted by extrapolation of the fitted curve to 50% lysis of hRBCs

51 Porter,E.A.; Weisblum,B.; Gellman,S.H. *J.Am.Chem.Soc.*, **2005**, *127*, 11516-11529.

52 Tossi,A.; Sandri,L.; Giangaspero,A. *Biopolymers*, **2000**, *55*, 1, 4-30

The ability of the peptides to disrupt the membrane integrity of mammalian cells was interrogated by a hemolysis assay with fresh human red blood cells (table 5). All peptide variants had increased hemolytic activity compared to mag2a, correlating with increased hydrophobicities.

2.4.3 Conclusions

To conclude, stapled mag2 showed significant enhancement in membrane-lytic activity in comparison with an unstapled one, and this facilitates stable pore formation in the membrane. For the first time, we have modified the on-membrane activity rather than binding affinity of mag2 by installing a staple into alpha-helical structure, which provides new insights into designing highly potent antimicrobial peptides. Additionally, to achieve maximal stabilization and thus highly potent mag2, we may incorporate a longer and more rigidified staple that can bridge sites far apart in amino acid sequence such as *i*, *i*+7 or even *i*, *i*+11. Staples with varied physical properties may also be interesting if we can introduce different staple into different position of peptide sequence. For example, we may put a more hydrophobic staple than triazole on the hydrophobic face of mag2.

Chapter 3: Conclusion

In summary, our goal is to enhance the selective toxicity of AMPs by chemical modifications, including incorporation of the photoisomerizable moiety azobenzene and environment-responsive residue LHA. Also we have studied the effect of a side-chain staple on the membrane-lytic activity of AMPs. Through these studies, we have gained useful information that may lead us to a better understanding of their mechanisms of actions, and shed a light on the future design and engineering AMPs as the novel antibiotic alternatives.

Development of mag2 with photo-switchable membrane-lytic activity has been achieved by incorporation of a photoisomerizable moiety azobenzene. Mechanistic studies suggest that the length of side chain plays an important role in the membrane-disturbing ability of mag2. In the second project, we tried to create a 'smart' mag2 only responsive to negatively charged membrane by incorporation of an environment-responsive LHA group. We got very limited success primarily due to the unexpected impact of negatively charged membrane on the pKa of this environment-responsive residue. We sacrificed bound peptide membrane-disturbing ability for increased difference in binding affinity, and eventually, we got only 2-fold increase in selectivity. However, incorporation of a side-chain staple into LHA carrying mag2 may help it to fold into the right structure and enhance function. Stapled mag2 showed significantly enhancement in membrane-disturbing ability in comparison with unstapled mag2 due to facilitated stable pores formation by stabilized α-helix on membrane.

AMPs provide an attractive platform to develop novel antibiotics because of their rapid-acting and special mechanisms of action. Through the fine-tuning of AMPs, specific antimicrobial and biological effects could be obtained such as specificity, stability, and toxicity. Here we present different strategies with the hope to apply them generally into other AMPs besides mag2 and use them widely as effective tools to explore their mechanism of action, and eventually, achieve the goal of developing a safe and effective therapeutic method to treat bacteria infections.

Materials and Methods

I. Materials and General Methods

N-Fmoc-*p*-amino-phenylalaine, Fmoc-Dap(Alloc)-OH and Boc-Phe(4-I)-OH were purchased from Chem-Impex International. Inc (Wood Dale, IL). All other Fmoc-protected amino acids were purchased from Advanced Chemtech (Louisville, KY). 1-palmitoyl-2-oleoyl-*sn*-glycerol-3-phosphocholine (POPC), 1-palmitoyl-2-oleoyl-*sn*-glycero-3-phospho- (1'-rac-glycerol) sodium salt (POPG), 1-palmitoyl-2-oleoyl-*sn*-glycero-3-phosphoethanolamine (POPE) were obtained from Avanti Polar Lipids (Alabaster, AL). Dansyl chloride and phenylsliane was purchased from Acros Organics (Geel, Belgium). All other chemical reagents were purchased from Sigma-Aldrich (Milwaukee, WI). Fmoc-OSu, Rink-Amide-MBHA resin, Fmoc-Ser(tBu)-Wang resin and O-Benzotriazole-N,N,N',N'-tetramethyl-uroniumhexafluoro-phosphate (HBTU) were purchased from Novabiochem (San Diego, CA).Peptide synthesis was carried out on a Tribute peptide synthesizer (Protein Technologies, Tucson, AZ). ^{1}H NMR and ^{13}C NMR data were collected on a Varian Gemini 400MHz NMR or Varian 500 MHz spectrometers. HR-MS data were generated by Boston College Mass-Spec facilities. Circular Dichroism measurements were performed on an Aviv 420 spectrometer (Biomedical, Inc., Lakewood, NJ). The protein concentration of all samples used in this study was determined by measuring their absorption on a Lambda 25 UV-Vis spectrometer (PerkinElmer, Waltham, MA). The extinction coefficient ε (330 nm) used for F12PAP-Mag2, F5DNS-F12PAP-Mag2, and F5W-F12PAP-Mag2 was 22387 $cm^{-1}M^{-}$

[1], 27687 $cm^{-1}M^{-1}$, 22387 $cm^{-1}M^{-1}$ respectively. For F5DNS-F12terphenyl-mag2, ε (280 jjnm) = 33800 $cm^{-1}M^{-1}$ and for other DNS incorporated peptides, ε = 4300 $cm^{-1}M^{-1}$. The LUVs were prepared by using Liposofast Mini Extrusion System (Avanti Polar Lipids, Alabaster, Alabama). Fluorescence measurements were all performed on a Fluorolog-3 fluorometer (Jobin Yvon Inc. Edison, NJ). Dynamic Light Scattering was performed on a DynaPro NanoStar (Wyatt Technology, Santa Barbara, CA).

II. Synthesis

(1) Preparation of Fmoc-phenylazophenylalanine-OH (Fmoc-PAP-OH)

Synthesis of Fmoc protected PAP was carried out via a modified procedure by Borisenko[53] *et at. N*-Fmoc-*p*-amino-phenylalaine (50 mg, 0.124 mmole) was dissolved in minimum amount of glacial acetic acid (5.5 mL). 3 equiv of nitrosobenzene (53 mg, 0.5 mmole) was added in and the mixture was stirred at room temperature overnight. The reaction mixture was then quenched with saturated sodium bicarbonate (15 mL) and extracted with ethyl acetate (3×30 mL). The combined organic layers was then dried with anhydrous Na_2SO_4 and concentrated on a rotary evaporator. The crude product was then purified by silica gel column chromatography (CH_2Cl_2/MeOH 9/1). The final product was obtained as an orange solid (55 mg, 90%); ESI+: MH^+ $C_{30}H_{26}N_3O_4$, calcd 492.1923, found 492.14636.

53 Borisenko, V.; Burns, D.C.; Zhang, Z.; Woolley, G.A. *J. Am. Chem. Soc.* **2000**, *122*, 6364-6370

(2) Preparation of (*S*)-3-([1,1':4',1''-terphenyl]-4-yl)-2-((*tert*-butoxycarbonyl)amino)propanoic acid (Boc-terphenyl-OH)

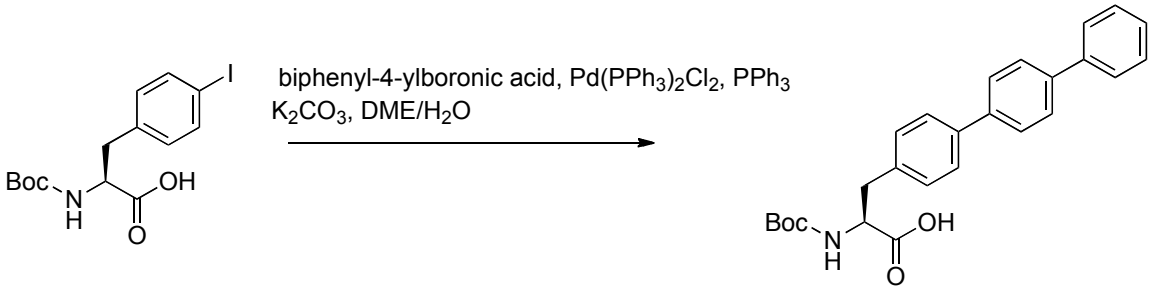

Scheme S1. Synthesis of Boc-terphenyl-OH

(S)-2-(tert-butoxycarbonylamino)-3-(4-iodophenyl) propanoic acid (500 mg), biphenyl-4-ylboronic acid (304 mg, 1.2 equiv.), $Pd(PPh_3)_2Cl_2$ (45 mg, 0.05 equiv.), PPh_3 (67 mg, 0.2 equiv.) and K_2CO_3 (353 mg, 2.0 equiv.) were mixed in a pressure vial. Under N_2 protection, 30 mL DME and 5 mL H_2O were added to dissolve all the solids and the resulting solution was sealed in the vial and stirred at 85 °C for ~1 hr. 1 N HCl was used to acidify the reaction to pH <1, and DCM was employed to extract the solution (3×). The combined organic layerS were washed with brine, dried over anhydrous Na_2SO_4, filtered, and the solvent was evaporated under vacuum. The crude product was purified by column chromatography on silica gel (toluene/HOAc 9/1) to afford the desired product (65%). ^{1}H NMR (500 MHz, Methanol–d_4) δ: 7.01-7.70 (m, 13H), 4.32 (m, 1H), 3.18 (m, 1H), 2.82 (m, 1H), 1.37 (s, 9H).

(3) Preparation of (*S*)-2-((((9*H*-fluoren-9-yl)methoxy)carbonyl)amino)-3-([1,1':4',1''-terphenyl]-4-yl)propanoic acid (Fmoc-terphenyl-OH)

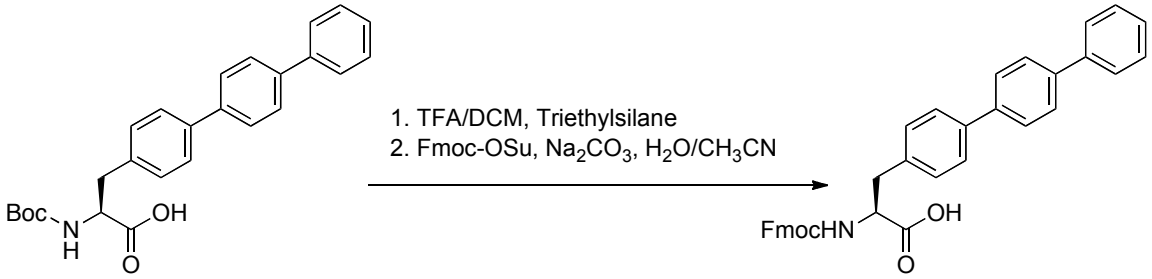

Scheme-S2. Synthesis of Fmoc-terphenyl-OH

Boc-terphenyl-OH **(**203 mg) was dissolved in 12 mL TFA/Et_3SiH mixture. After stirring at room temperature for 0.5 hr, the solvent was evaporated under vacuum. Then 20 mL of 10% Na_2CO_3 and 12 mLCH_3CN was used to dissolve the residue, with Fmoc-OSu (148 mg, 0.9 equiv.) addition. The mixture was stirred vigorously at room temperature for 2.5 hrs. The reaction was quenched with 2 N HCl and extracted with DCM (3×). The combined organic layers were dried over Na_2SO_4, filtered, and concentrated under vacuum. The crude material was purified by flash column chromatography on silica gel (Toluene/HOAc 15/1) to give the desired product as a white solid (90%). ^{1}H NMR (500 MHz, Chloroform–*d*) δ: 7.77 (d, J = 7.5 Hz, 2H), 6.84-7.66 (m, 19H), 4.42 (m, 1H), 3.25 (m, 1H), 3.10 (m, 1H).

(4) Preparation of *(S)*-methyl 2-(tert-butoxycarbonylamino)-4-(tosyloxy)butanoate

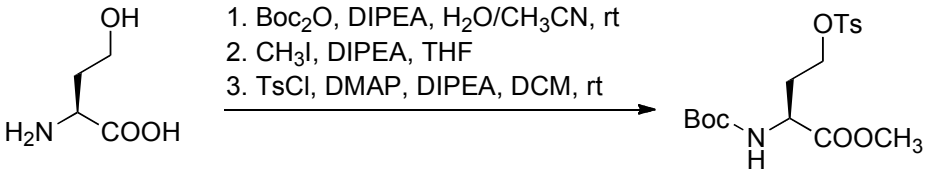

Scheme S3. Synthesis of *(S)*-methyl 2-(tert-butoxycarbonylamino)-4-(tosyloxy)butanoate

(S)-2-amino-4-hydroxybutanoic acid (1.0 g) was suspended in a solution of 2.93 mL (2.0 equiv.) N, N-Diisopropylethylamine in 60 mL acetone/CH_3OH (9:1). Then Di-*tert*-butyl dicarbonate (2.02 g, 1.1 equiv.) was added in portions. The resulting mixture was stirred at room temperature for 16 hrs. All solvents and excess reagent were removed under vacuum, and the obtained white solid was directly used in the next step. To a slurry of this compound in 50 mL THF was added (1.9 mL, 1.3 equiv.) N, N-Diisopropylethylamine, followed by an addition of (1.05 mL, 2.0 equiv.) CH_3I. The resulting mixture was stirred at room temperature overnight. The solvent was removed under vacuum and the residue was treated with 1 N HCl solution, and then extracted with EtOAc three times. The combined organic layers were washed with brine, dried over Na_2SO_4, filtered, and concentrated to afford a crude material that was used directly in the following step. DMAP (26 mg, 0.1 equiv.) was added to a solution of 500 mg crude material, *p*-Toluenesulfonic anhydride (841mg, 1.2 equiv.) and 486 μl DIPEA in DCM at 0 ^oC. After the resulting mixture was stirred at room temperature for 24 hrs, it was poured into 50 mL 1 N HCl solution, and extracted with DCM (3×). The combined organic layers were washed with brine, dried over Na_2SO_4, filtered, and concentrated. The crude

product was then purified with silica gel column (hexane/Et_2O 1/1) to yield a colorless crystal (combined yield 40%). ^{1}H NMR (500 MHz, Chloroform–*d*) δ: 7.78 (d, J = 6.5 Hz, 2H), 7.36 (d, J = 9.0 Hz, 2H), 5.17 (d, J = 8.5 Hz, 2H), 4.33 (m, 1H), 4.11 (m, 2H), 3.71 (s, 3H), 2.45 (s, 3H), 2.21 (m, 1H), 2.11 (m, 1H), 1.42 (s, 9H).

(5) Preparation of (*S*)-methyl 2-((*tert*-butoxycarbonyl)amino)-4-((2,6-dimethylpyridin-4-yl)oxy)butanoate

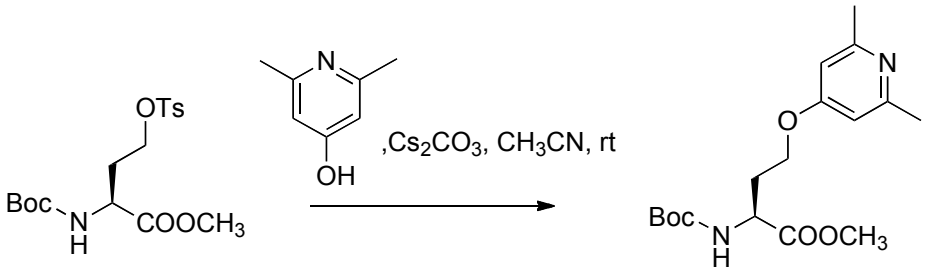

Scheme S4. Synthesis of (*S*)-methyl 2-((*tert*-butoxycarbonyl)amino)-4-((2,6-dimethylpyridin-4-yl)oxy)butanoate (Boc-LHA-COOMe)

(S)-methyl 2-(tert-butoxycarbonylamino)-4-(tosyloxy)butanoate (100 mg), Cs_2CO_3 (168mg, 2.0 equiv.) and 2,6-dimethylpyridin-4-ol (54 mg, 1.7 equiv.) were mixed in 10 mL CH_3CN, and the resulting mixture was stirred at room temperature for 4 hrs. The reaction was treated with a mixture of saturated $NaHCO_3$ solution and water to pH > 9,

and extracted with DCM (3×). The combined organic layers were washed with brine, dried over Na_2SO_4, filtered, and concentrated under vacuum. The crude material was purified by flash column chromatography on silica gel (EtOAc) to give the desired product (92%). ^{1}H NMR (500 MHz, Chloroform–*d*) δ: 6.46 (s, 2H), 5.31 (d, *J*= 6.0 Hz, 1H), 4.50 (m, 1H), 4.07 (t, *J*= 6.0 Hz, 2H), 3.77 (s, 3H), 2.46 (s, 6H), 2.33 (m, 1H), 2.23 (m, 1H), 1.44 (s, 9H).

(6) Preparation of (S)-2-(((9H-fluoren-9-yl)methoxy)carbonylamino)-4-(2,6-dimethylpyridin-4-yloxy)butanoic acid (Fmoc-LHA-OH)

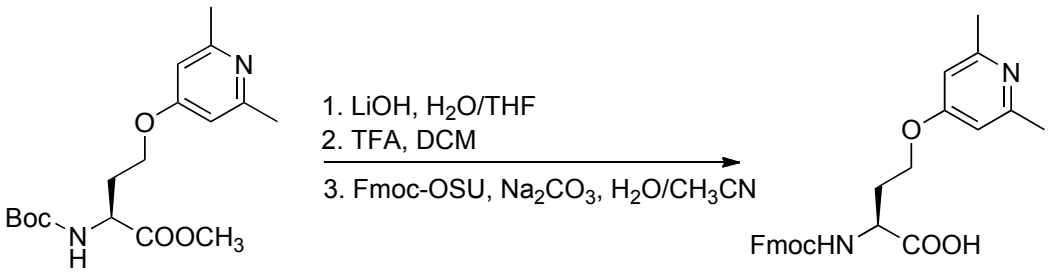

Scheme S5. Synthesis of Fmoc-LHA-OH

(*S*)-methyl 2-((*tert*-butoxycarbonyl)amino)-4-((2,6-dimethylpyridin-4-yl)oxy)butanoate (72 mg) was dissolved in 1 mL THF, then 3 mL H_2O and LiOH•H_2O (45 mg, 5.0 equiv.)

were added. The resulting solution was stirred at room temperature for 36 hrs. 1 N HCl was added to tune the pH to 5-7, and all solvents were removed under vacuum. 5 mLTFA and 250 μL Et_3SiH were then added to the residue and stirred at room temperature for 2 hrs. Solvents were then removed under vacuum, and the residue was treated with 4 mL 10% Na_2CO_3 solution and 2mL CH_3CN, then Fmoc-OSu (65 mg, 0.9 equiv.) was added. The resulting mixture was stirred at room temperature vigorously for 2.5 hrs. The reaction was quenched with 15 mL 1 N HCl solution and extracted with DCM (6×). The combined organic layers were dried over Na_2SO_4, filtered, and concentrated. The crude product was obtained through column chromatography purification on silica gel as a yellow oil (90%). ^{1}H NMR (500 MHz, Methanol–d_4) δ: 7.78 (d, J = 7.5 Hz, 2H), 7.66 (m, 2H), 7.41 (m, 2H), 7.32 (m, 2H), 7.30 (s, 2H), 4.29-4.48 (m, 5H), 4.11 (m, 1H), 2.6 (s, 6H), 2.47 (m, 1H), 2.23 (m, 1H).

(7) Preparation of (S)-methyl 2-acetamido-4-(2,6-dimethylpyridin-4-yloxy)butanoate

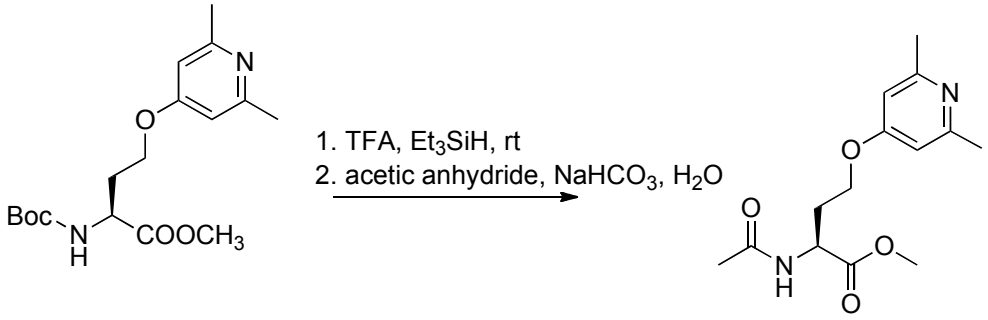

Scheme S6. Synthesis of (S)-methyl 2-acetamido-4-(2,6-dimethylpyridin-4-yloxy)butanoate

(*S*)-methyl 2-((*tert*-butoxycarbonyl)amino)-4-((2,6-dimethylpyridin-4-yl)oxy)butanoate (150 mg) were dissolved in 8 mL TFA and 0.4 mL Et_3SiH, and the resulting mixture was stirred at room temperature for 2.5 hrs. The solvent was removed under vacuum and a mixture of saturated $NaHCO_3$ solution and water was added to tune the pH to 5-7. Acetic anhydride (63 μL, 1.5 equiv.) was added then and the resulting solution was stirred at room temperature overnight. 10% Na_2CO_3 was employed to tune the pH to 10-12 and DCM was used for extraction (3×). The combined organic layers were dried over Na_2SO_4, filtered, and concentrated. The crude product was obtained through column chromatography purification on silica gel (DCM/Methanol 9/1) as a colorless oil (92%). ^{1}H NMR (500 MHz, Chloroform–*d*) *δ*: 6.44 (s, 2H), 4.76 (m, 1H), 4.05 (m, 2H), 3.77 (s, 3H), 2.47 (s, 6H), 2.39 (m, 1H), 2.27 (m, 1H), 2.04 (s, 3H). ^{13}C NMR (100 MHz, Chloroform–*d*) *δ*: 172.5, 170.2, 159.2, 106.6, 63.7, 52.6, 50.0, 31.2, 24.4, 23.0. HRMS (ESI+): *m/z* calculated for $C_{14}H_{21}N_2O_4$ $[M]^+$, 281.15013; found 281.15080.

(8) Preparation of 4-(dodecyloxy)-2,6-dimethylpyridine

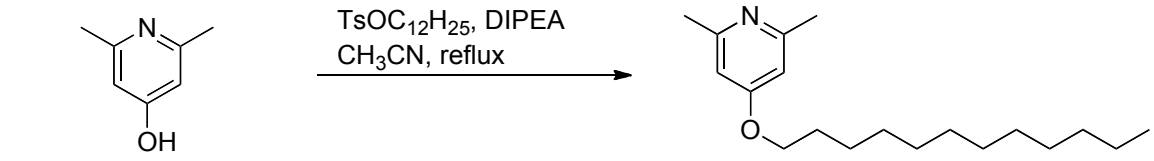

2,6-dimethylpyridin-4-ol

4-(dodecyloxy)-2,6-dimethylpyridine

Scheme S7. Synthesis of 4-(dodecyloxy)-2,6-dimethylpyridine

2,6-dimethylpyridin-4-ol (123 mg), dodecyl 4-methylbenzenesulfonate (343 mg, 1.2 equiv.) and DIPEA (258mg, 2.0 equiv.) were mixed in 10 mL CH_3CN. After the resulting solution was refluxed overnight, all the solvent was evaporated under vacuum. The residue was resuspended in 10% Na_2CO_3 solution and extracted with DCM (3×). The combined organic layers were dried over anhydrous Na_2SO_4, filtered, and evaporated under vacuum. The crude material was purified through flash column chromatography on silica gel (EtOAc) to yield the desired product as a colorless liquid (80%). ^{1}H NMR (500 MHz, Chloroform–*d*) δ: 6.48 (s, 2H), 3.95 (t, *J=6.5*Hz, 2H), 2.46 (s, 6H), 1.78 (m, 2H), 1.42 (m, 2H), 1.26 (m, 16H), 0.88 (t, *J*=7.0Hz, 3H). ^{13}C NMR (100 MHz, Chloroform–*d*) δ: 158.9, 106.5, 67.5, 31.8, 29.5, 29.5, 29.5, 29.4, 29.2, 29.2, 29.1, 28.9, 26.0, 24.4, 22.6, 14.0. HRMS (ESI+): *m/z* calculated for $C_{19}H_{34}N_1O_1$ $[M]^+$, 292.26404; found 292.26525.

(9) Preparation of NBD-POPE

The synthesis of NBD-POPE was performed according to a published procedure[54] except that NBD-F was used instead of NBD-Cl. The obtained product (quantitative yield) was dissolved in anhydrous chloroform and kept at -30°C.

(10) Preparation of Fmoc-Nle (εN_3)-OH

Fmoc-Nle (εN_3)-OH was prepared from Fmoc-Lys-OH by a published method[55]. Sodium azide reacted with triflic anhydride to generate triflyl azide, which was directly used in

[54] Frazier, M.L.; Wright, J.R.; Pokorny, A.; and Almeida, P.F.F. *Biophys. J.* **2007**, *92*, 2422
[55] Katayama, H.; Hojo, H.; Ohira, T.; Nakahara, Y. *Tetrahedron Letters*, **2008**, *49*, 5492-5494

the copper (II)-catalyzed diazo transfer reaction with Fmoc-Lys-OH, leading to the final product as a off-white solid (84%).

(11) Preparation of F12PAP-mag2&F5W-F12PAP-mag2

Peptides were synthesized through Fmoc/tBu chemistry with the Fmoc-Ser (tBu)-Wang resin as the solid support. The synthesis was carried out on 0.05 mmole scale. Five equivalents of the commercially available amino acids as well as the synthetic PAP were used for the coupling reaction. The peptides were cleaved off the resin and deprotected with reagent K (80% TFA, 5% H2O, 2.5% EDT, 5% Thioanisole and 7.5% Phenol). The crude products were purified by RP-HPLC (Waters Prep LC, Jupiter 10u C4 300A Column).

(12) Preparation of F5DNS-F12PAP-mag2

Fmoc-Dap (Alloc)-OH and PAP were incorporated into the peptide sequence to replace the 5^{th} and 12^{th} phenylalanine respectively, following the same procedures as other natural amino acids did through Fmoc/tBu chemistry with the Fmoc-Ser (tBu)-Wang resin as the solid support. However, there was no N-terminal Fmoc group removal step, and the N-terminal glycine was introduced via an *N*-a-Boc-protected one in order to yield a free N-terminal a-amino group after final protecting group removal and resin cleavage. The Alloc deprotection was accomplished by addition of Pd $(PPh_3)_4$ (0.8 equivalent),

phenylsilane (25 equivalents) into the suspension of resin-bound peptide in dry CH_2Cl_2 (30 mM in peptide), followed by shaking under nitrogen protection for 15min[56]. To guarantee the efficiency, the deprotection was repeated two additional times. Te dansyl residue was directly incorporated by reaction of the free amine (12.5 mM in DMF) with dansyl chloride (3 equivalents) and *N, N*-Diisopropylethylamine (6 equivalents) at room temperature stirring overnight. The peptides were cleaved off the resin and deprotected with reagent K (80% TFA, 5% H2O, 2.5% EDT, 5% Thioanisole and 7.5% Phenol). The crude products were purified by RP-HPLC (Waters Prep LC, Jupiter 10u C4 300A Column).

(13) Preparation of F5DNS-F12Bipheyl-Mag2 & F5DNS-F12Terphenyl-Mag2

These two peptides were synthesized by the same methods described in (6), except for the substitution at 12th phenylalanine was Fmoc-Ala (4,4'-biphenyl)-OH and Fmoc-Terphenyl-OH respectively.

56 Sainlos, M.; Imperiali, B. *Nat. Protoc.* **2007**, *2*, 3201.

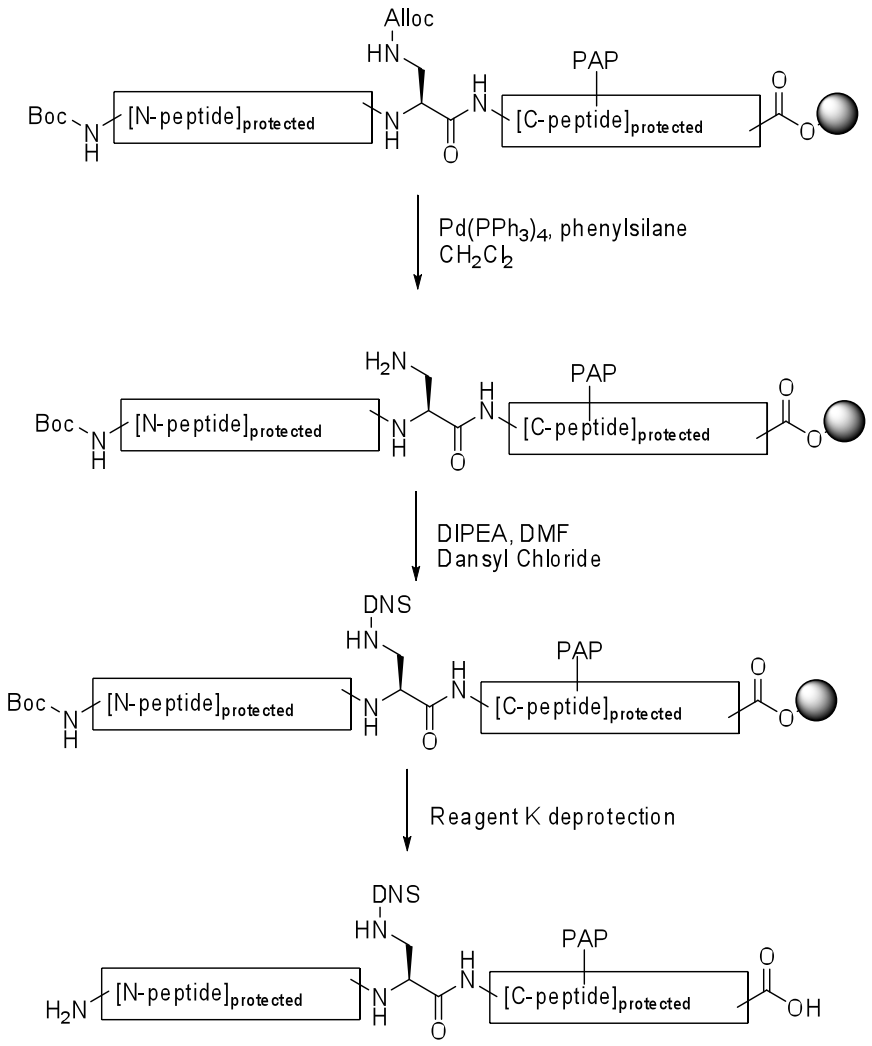

Scheme-S8. Synthesis of F5DNS-F12PAP-mag 2

(14) Preparation of N-DNS-mag2a, N-DNS-F12LHA-mag2a & N-DNS-TriLHA-mag2a

All peptides were synthesized on Rink-Amide-MBHA resin (90 mg, 0.56 mmol/g, 0.05 mmol) using standard Fmoc/HBTU chemistry. Five equivalents of the commercially available amino acids were used for the coupling reaction. The incorporation of the LHA

moiety was accomplished by using three equivalents of the Fmoc-LHA-OH and extended coupling time (1 hour). After cleavage of the N-terminal Fmoc group from the fully protected peptide on resin, a dansyl residue was attached by the reaction of the N-terminal amino group with dansyl chloride (40 mg, 0.15 mmol) in presence of DIPEA (52 mL, 0.30 mmol) overnight. The cleavage and purification steps were the same as other peptide synthesis described above.

(15) Preparation of linear mag2a

Linear precursor synthesis was carried out according to the same procedure in (9). For the azide and terminal alkynyl moiety incorporation, three equivalents of the Fmoc-Nle (εN_3)-OH and Fmoc-propargylglycine (Pra) were used with an extended coupling time (1 hr). The cleavage and purification steps were the same as other peptide synthesis described above.

(16) Preparation of stapled mag2a

Cyclization of the purified linear precursor was carried out under the condition published by Cantel *et al.*[57], which employed 4.4 equivalents of $CuSO_4$ and ascorbic acid with a peptide concentration of 1mg/ml in 2:1 H_2O/*t*-BuOH. The reaction was monitored by analytical RP-HPLC. The reaction went to a completion within 1 hr at room temperature. After the conversion was done, organic solvent was evaporated and the residue was lyophilized to afford the crude product, which then was resuspended and purified with RP-HPLC.

---

[57] Cantel, S.; Isaad Ale, C.; Scrima, M.; Levy, J. J.; DiMarchi, R. D.; Rovero, P.; Halperin, J. A.; D'Ursi, A. M.; Papini, A. M.; Chorev, M. *J Org Chem* **2008**, *73*, 5663.

III Measurements

(1) Vesicle preparation

Lipids mixture with the desired compositions was dissolved in chloroform. The solution was dried under a high vacuum overnight. The lipid films were then dispersed in TES buffered solution (10 mM 2-[Tris(hydroxymethyl)methylamino]-1-ethanesulfonic acid, 100 mM sodium citrate, pH = 7.0) to a final lipid concentration of 100 mM. The lipid suspension was freeze-thawed for 20 cycles and extruded through filters (20 times) whose pore size was 100 nm. The mean diameter of the LUVs was determined by dynamic light scattering to be 65-75 nm. SUVs for CD spectroscopy were prepared by sonication of the lipid suspension in buffer (10 mM Trizma, 150 mM NaCl, pH=7.0) using a titanium-tipped ultrasonicator. The lipid concentration was determined in triplicate based on complex formation between ammonium ferrothiocyanate and POPC according to stewart assay[58].

(2) Liposome leakage assay

Tb^{3+} entrapped LUVs were prepared by hydrating a desired lipids mixture with Tb^{3+} solution (50 mM Tb^{3+}, 10mM TES, 100 mM Sodium citrate, pH=7). After extrusion as described above, Tb^{3+} entrapped LUVs were separated from free Tb^{3+} on a Bio-Gel A1.5m column immediately. The release of Tb^{3+} from the LUVs formed Tb^{3+}/DPA complex and was fluoremetrically monitored at an excitation wavelength of 270 nm and an emission wavelength of 489 nm at 25 ^{o}C.

[58] Stewart, J.C.M. *Analytical Biochemistry*, **1980**, *104*, 10-14

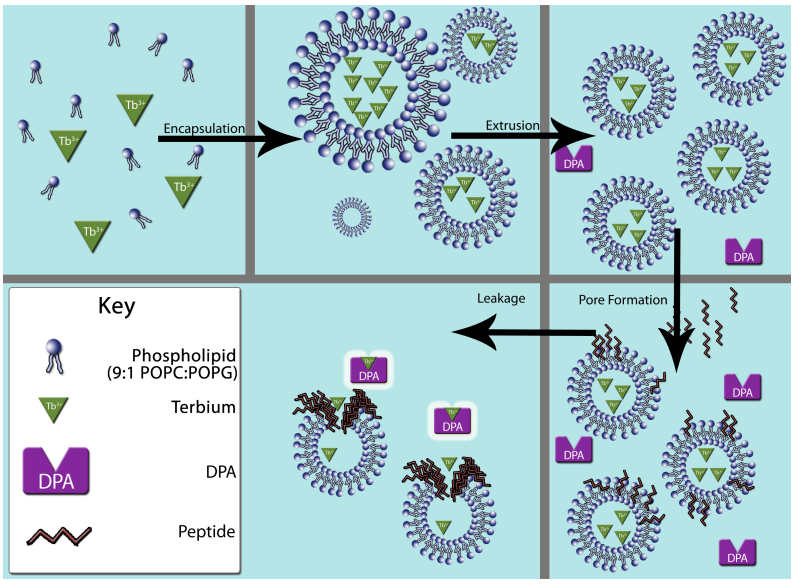

Scheme S9. Tb^{3+}/DPA complex based leakage assay

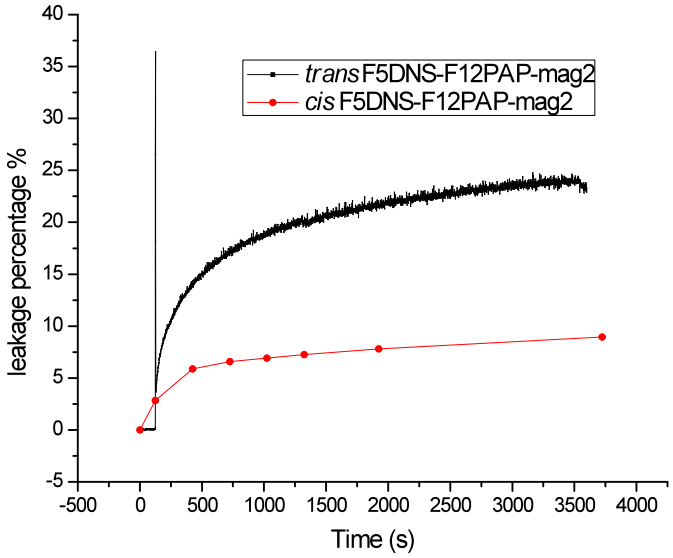

Figure S1. Photoswitching modulates F5DNS-F12PAP-mag2 membrane permeabilization. This experiment was performed with 1 μM peptide and 500 μM LUVs made of POPC/POPG 1/1 at room temperature with stirring.

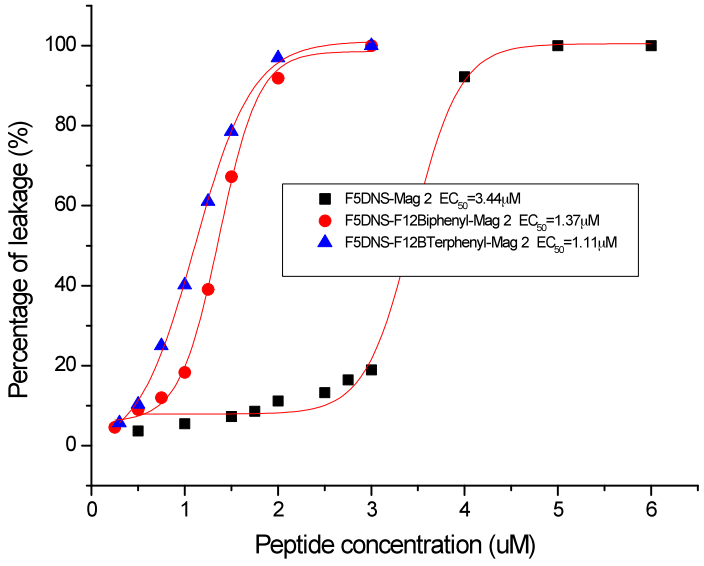

Figure S2. EC_{50} determination of F5DNS-mag2, F5DNS-F12biphenyl-OH and F12terphenyl-OH. This experiment was performed with 500 μM LUVs (POPC/POPG 1/1) and varying concentrations of peptides.

(3) CD spectroscopy

CD measurements of all mag2 mutants were performed with peptides in the presence of SUVs (POPC: POPG=1:1) or 50% TFE in PBS buffer at room temperature. For each spectrum, three scans were accumulated and the baseline (SUVs without peptide) was subtracted.

(4) Binding affinity assay

The binding affinity of the peptides against the membrane was determined on the basis of dansyl fluorescence. Peptide solutions were incubated with various amounts of LUVs (POPC/POPG 1/1 or POPC) at 25 °C until no more change of dansyl fluorescence was observed. Fluorescence spectra in the range of 490-570 nm were recorded at an excitation

wavelength of 337 nm. The spectra were corrected by subtraction of corresponding blank spectra without the peptide.

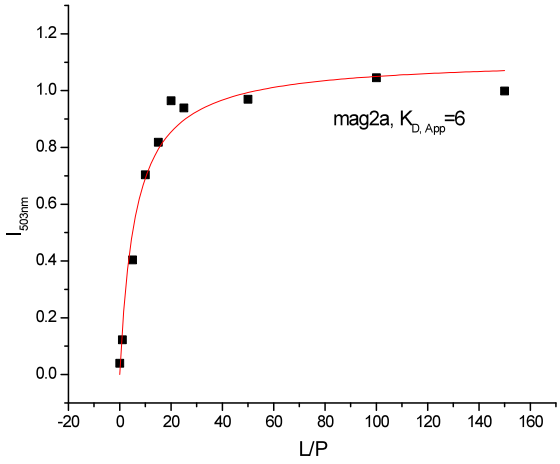

Figure S3. Binding affinity of mag2a towards LUVs POPC/POPG 1/1. This experiment was performed with 4 μM peptide and varying concentrations of lipids.

(5) Peptide translocation measurement

Peptide was incubated with LUVs at 30 ^{o}C for 2 hrs. For 2 μM peptide in 2 mL solution, 14 mL of a trypsin solution (5 mg/mL in 1 mM HCl) was added to hydrolyze the peptide molecules located on the outer leaflet. The dansyl fluorescence was monitored and no more decrease at 505 nm was observed after 20 min. This value was recorded as F_m.

(6) NBD quenching assay

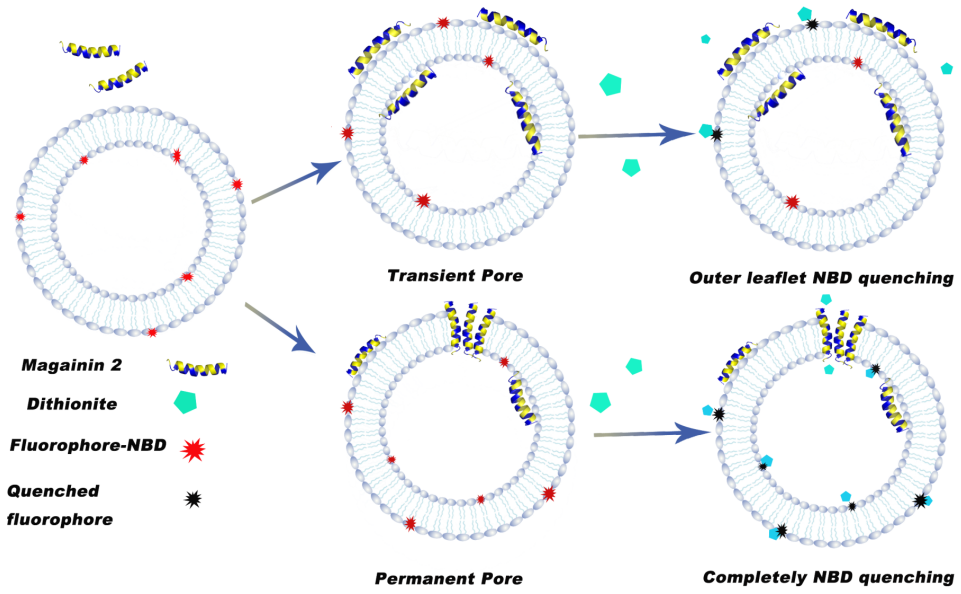

Scheme S10. Fluorescence quenching assay

(7) Antimicrobial Activity

Antimicrobial activity was measured as Minimal Inhibitory Concentrations (MICs) against both Gram-negative *Escherichia Coli* (BL21) and Gram-positive *Bacillus subtilis* (ATCC 663) using broth microdilution method. Bacteria from a single colony were grown overnight in LB broth at 37 °C with agitation. An aliquot was taken and diluted in fresh broth and cultured for another ~ 2 hours until the cells reached mid-logarithmic phase (OD_{590} ~ 0.5). The cells were then diluted to a concentration of ~ 5×10^5 colony forming units/mL and 200 μL of the diluted solution was added to each well of a sterile 96-well plate. 2 μL of serial dilution (2-fold) of peptides in DMSO were added in triplicate. The plate were mixed for 30 seconds, followed by incubation at 37°C for 18

hrs. The absorbance at 590 nm was monitored using a microtiter plate reader SpectraMax M5, Molecular Devices, Sunnyvale, CA). The MIC was recorded as the minimum concentration of peptides required for the complete inhibition of cell growth (no change in absorbance).

(8) Hemolytic assay

Fresh type B human blood cells (hRBCs) were centrifuged at 3500 rpm and washed with PBS buffer until the supernatant was clear. The hRBCs were then resuspended and diluted to a final concentration of 1% (v/v) in PBS and used immediately. 15 μL of serial dilution (2-fold) of peptides in DMSO or DMSO only as negative control was added to 1.5 mL of hRBCs in PBS. The resulted mixture was gently shaken to mix well and incubated at 37 °C for 1 hr, followed by centrifugation at 3500 rpm for 10 min using tabletop centrifuge. An aliquot (50 μL) of supernatant in triplicate was transferred to a sterile 96-well plate containing 50 μL of H_2O in each well. Release of hemoglobin was monitored at 415 nm using a microtiter plate reader. Percentage hemolysis was calculated using percentage hemolysis = $100 \bullet (A_{415,\ peptide} - A_{415,\ DMSO}) / (A_{415,\ complete\ hemolysis} - A_{415,\ DMSO})$, where complete hemolysis is achieved by mixing hRBCs with 1% TritonX-100.

(9) pKa measurement

The UV-Vis spectrum of LHA moiety differs at different pH: The maximum absorbance shifts from 238 nm to 225 nm when LHA switches from protonated form to depronated form. pKa of LHA moiety in PBS buffer was measured with (S)-methyl 2-acetamido-4-(2,6-dimethylpyridin-4-yloxy)butanoate **1**. The concentration of **1** was 2 mM. The pH

was determined by a glass electrode (Thermal Fisher Scientific, Beverly, MA) relative to NBS standard solutions.

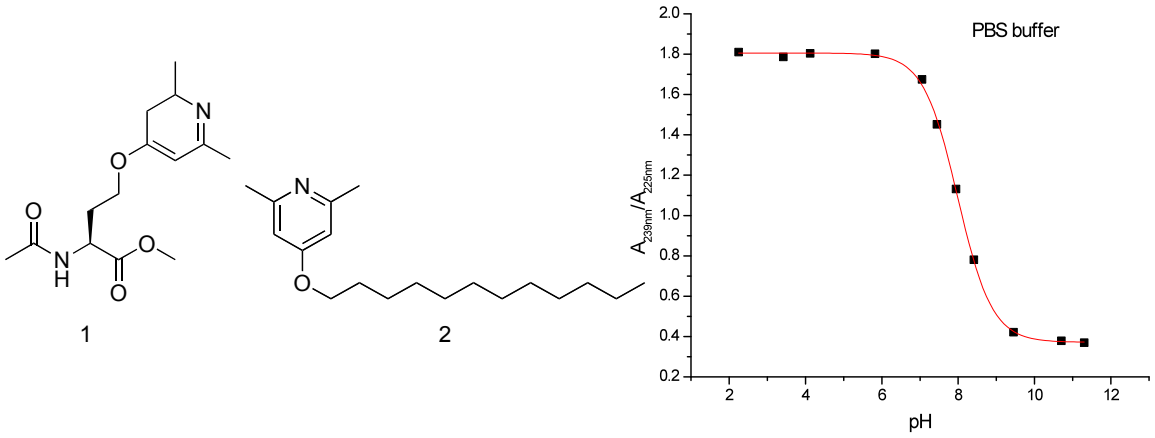

Figure S4. pKa measurement of LHA in aqueous solution

pKa of LHA moiety in membrane was measured with 4-(dodecyloxy)-2,6-dimethylpyridine **2** in micellar solutions of sodium dodecyl sulfate (SDS) and dodecylphosphocholine (DPC). The detergent concentrations were 20 mM for SDS and Triton X-100. The titration was performed in the presence of PBS buffer.

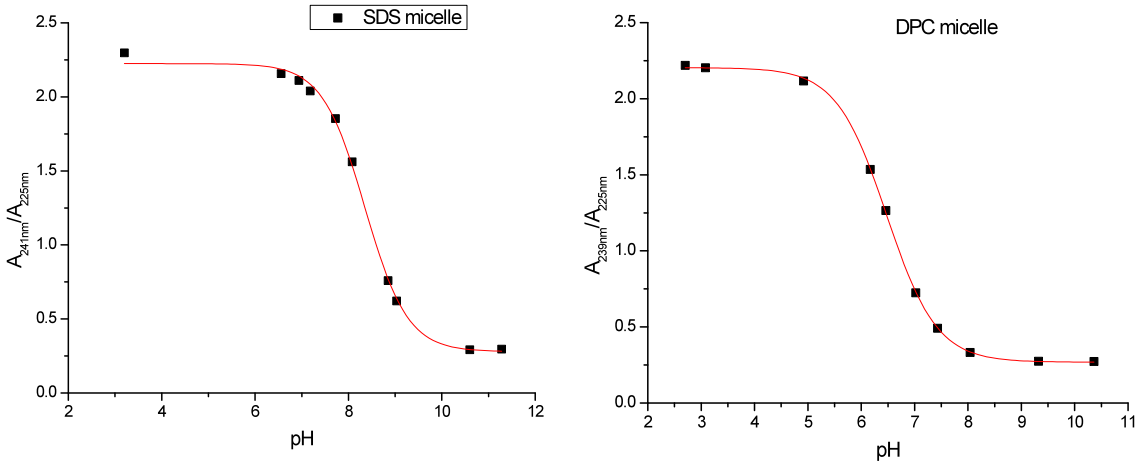

Figure S5. pKa measurement of LHA in membranes

Appendix

Peptide	Sequence
F12PAP-mag2	GIGKFLHSAKK(PAP)GKAFVGEIMDS
F5DNS-F12PAP-mag2	GIGK(DNS)LHSAKK(PAP)GKAFVGEIMDS
F5W-F12PAP-mag2	GIGKWLHSAKK(PAP)GKAFVGEIMDS
F5DNS-mag2	GIGK(DNS)LHSAKKFGKAFVGEIMDS
F5DNS-F12Biphenyl-mag2	GIGK(DNS)LHSAKK(Bipheyl)GKAFVGEIMDS
F5DNS-F12Terphenyl-mag2	GIGK(DNS)LHSAKK(Terphenyl)GKAFVGEIMDS
N-DNS-mag2a	DNS-GIGKFLHSAKKFGKAFVGEIMDS-NH_2
N-DNS-TriLoHoAla-mag2a	DNS-GIGK(LHA)LHSAKK(LHA)GKA(LHA)VGEIMDS-NH_2
N-DNS-F12LoHoAla-mag2a	DNS-GIGKFLHSAKK(LHA)GKAFVGEIMDS-NH_2
Mag2a	DNS-GIGKFLHSAKKFGKAFVGEIMNS-NH_2
Mag2a-1 (linear)	DNS-GIGKFLHSAK(Nle)FGK(Pra)FVGAIMNS-NH_2
Mag2a-1S (cross-linked)	DNS-GIGKFLHSAK(Nle)FGK(Pra)FVGAIMNS-NH_2
Mag2a-2 (linear)	DNS-GIGKFLHS(Nle)KKF(Pra)KAFVGEIMNS-NH_2
Mag2a-2S (cross-linked)	DNS-GIGKFLHS(Nle)KKF(Pra)KAFVGEIMNS-NH_2